AGU PUBLICATIONS

JGR

Journal of Geophysical Research: Atmospheres

RESEARCH ARTICLE
10.1002/2016JD025979

Key Points:
- CMIP5 models represent the interannual NAO pattern reasonably well but the decadal NAO pattern less well
- Multidecadal fluctuations of the NAO and the internal NHT are generally underestimated by CMIP5 models
- CMIP5 model representation of the NAO-NHT relationship depends on their interpretation of the oceanic processes related to the AMOC

Correspondence to:
J. Li and C. Sun,
ljp@bnu.edu.cn;
scheng@bnu.edu.cn

Citation:
Wang, X., J. Li, C. Sun, and T. Liu (2017), NAO and its relationship with the Northern Hemisphere mean surface temperature in CMIP5 simulations, *J. Geophys. Res. Atmos.*, *122*, 4202–4227, doi:10.1002/2016JD025979.

Received 23 SEP 2016
Accepted 25 MAR 2017
Accepted article online 28 MAR 2017
Published online 25 APR 2017

NAO and its relationship with the Northern Hemisphere mean surface temperature in CMIP5 simulations

Xiaofan Wang[1,2], Jianping Li[3,4], Cheng Sun[3], and Ting Liu[5]

[1]State Key Laboratory of Numerical Modeling for Atmospheric Sciences and Geophysical Fluid Dynamics, Institute of Atmospheric Physics, Chinese Academy of Sciences, Beijing, China, [2]College of Earth Sciences, University of Chinese Academy of Sciences, Beijing, China, [3]State Key Laboratory of Earth Surface Processes and Resource Ecology and College of Global Change and Earth System Science, Beijing Normal University, Beijing, China, [4]Laboratory for Regional Oceanography and Numerical Modeling, Qingdao National Laboratory for Marine Science and Technology, Qingdao, China, [5]State Key Laboratory of Satellite Ocean Environment Dynamics, Second Institute of Oceanography, State Oceanic Administration, Hangzhou, China

Abstract The North Atlantic Oscillation (NAO) is one of the most prominent teleconnection patterns in the Northern Hemisphere and has recently been found to be both an internal source and useful predictor of the multidecadal variability of the Northern Hemisphere mean surface temperature (NHT). In this study, we examine how well the variability of the NAO and NHT are reproduced in historical simulations generated by the 40 models that constitute Phase 5 of the Coupled Model Intercomparison Project (CMIP5). All of the models are able to capture the basic characteristics of the interannual NAO pattern reasonably well, whereas the simulated decadal NAO patterns show less consistency with the observations. The NAO fluctuations over multidecadal time scales are underestimated by almost all models. Regarding the NHT multidecadal variability, the models generally represent the externally forced variations well but tend to underestimate the internal NHT. With respect to the performance of the models in reproducing the NAO-NHT relationship, 14 models capture the observed decadal lead of the NAO, and model discrepancies in the representation of this linkage are derived mainly from their different interpretation of the underlying physical processes associated with the Atlantic Multidecadal Oscillation (AMO) and the Atlantic meridional overturning circulation (AMOC). This study suggests that one way to improve the simulation of the multidecadal variability of the internal NHT lies in better simulation of the multidecadal variability of the NAO and its delayed effect on the NHT variability via slow ocean processes.

1. Introduction

The North Atlantic Oscillation (NAO) is one of the most prominent modes of atmospheric variability over the Northern Hemisphere (NH) and has an important influence on the climate of the North Atlantic and surrounding continents [*Hurrell*, 1995; *Hurrell et al*., 2003]. The spatial structure of the NAO is characterized by the opposite variation of two pressure centers, the Azores High and the Icelandic Low, reflecting atmospheric mass fluctuation between the midlatitudes and the polar region [*Hurrell*, 1995; *Thompson and Wallace*, 2001; *Li and Wang*, 2003]. The temporal variability of the NAO covers time scales ranging from interannual to interdecadal [*Wanner et al*., 2001; *Li and Wang*, 2003; *Li et al*., 2013; *Sun et al*., 2015b]. Accordingly, the NAO makes an important contribution to climate variability over different time scales [*Hurrell and Van Loon*, 1997; *Gong et al*., 2001; *Ding et al*., 2005; *Li*, 2005; *Deser and Teng*, 2008; *Wu et al*., 2009, 2012; *Sun et al*., 2015a; *Zheng et al*., 2016].

The NH mean surface temperature (NHT) shows a well-defined multidecadal variability during the twentieth century [*Schlesinger and Ramankutty*, 1994; *Swanson et al*., 2009; *Li et al*., 2013]. Many studies have tried to identify the source of this multidecadal variability and attributed it to both external forcings [*Stott et al*., 2000; *Booth et al*., 2012] and internal climate variability [*Delworth and Mann*, 2000; *Zhang et al*., 2007; *Li et al*., 2013; *Dai et al*., 2015]. Recently, *Li et al*. [2013] found that the preceding NAO may be an important source of the multidecadal variability of the NHT. They found observational evidence that the NAO leads the detrended NHT by about 16 years and also that the Atlantic Multidecadal Oscillation (AMO), as well as the associated slow ocean processes, may play an important role in connecting the multidecadal variability of the NAO with that of the NHT. Their study assists our understanding of internal climate change over

multidecadal scales, as well as improving the interpretation and projection of the NHT changes in climate models. Thus, it is necessary to examine how the NAO variability and its connection to the NHT over multidecadal time scales are represented in climate models.

The Coupled Model Intercomparison Project (CMIP) provides us with a unique opportunity to evaluate the skill of coupled models in reproducing NAO variability and its climatic impact. In fact, the representation of the spatial and temporal variability of the NAO by climate models has been analyzed in earlier studies. Previous assessments of the models that participated in phase 3 of the CMIP (CMIP3) have shown that the main features of the seasonal [*Stoner et al*., 2009; *Bladé et al*., 2012; *Handorf and Dethloff*, 2012] and daily [*Casado and Pastor*, 2012] spatial patterns of the NAO are captured by most models. However, most of the CMIP3 models fail to capture the spectral behavior [*Stoner et al*., 2009; *Handorf and Dethloff*, 2012] of the NAO. In addition, *Casado and Pastor* [2012] suggested that although some of the CMIP3 models were able to reproduce the characteristics of the probability distribution of the daily NAO, none of them could properly reproduce the NAO's characteristic time scales. *Keenlyside et al*. [2008] found that the temporal evolution of the NAO over multidecadal time scales simulated by ECHAM5/MPI-OM (one of the CMIP3 models) did not agree with the observations. They pointed out that this might be a possible source of bias in the decadal climate predictions, as the NAO is an important atmospheric forcing over multidecadal time scales. However, their study involved only one model, and it is necessary to further assess how the NAO multidecadal variability is represented in other CMIP models.

Phase 5 of the CMIP (CMIP5) contains more models with a generally higher spatial resolution than did CMIP3 [*Taylor et al*., 2012], and this provides us with a better chance to understand NAO variability and its climatic impacts. Recently, *Lee and Black* [2013] identified NAO-like patterns within the CMIP5 simulations and assessed the correspondence between model simulations and reanalysis data using cluster analysis. They found that a minority of models failed to replicate the NAO pattern and that their inability to simulate the NAO pattern may have been derived from their inadequate interpretation of climatological stationary waves. *Davini and Cagnazzo* [2013] analyzed the representation of the wintertime NAO in CMIP5 simulations and pointed out a possible misinterpretation of the empirical orthogonal function (EOF)-based NAO pattern caused by model biases in the underlying dynamical processes related to atmospheric blocking. *Gillett and Fyfe* [2013] studied the historical and future trends of the NAO simulated by the CMIP5 models and the NAO response to volcanic aerosols and solar irradiance. However, none of these studies considered the performance of models in describing the spatial or temporal variability of the NAO over multidecadal time scales.

In this paper, we address two main issues. First, we systematically analyze the spatial pattern and temporal variability of the NAO, with special focus on multidecadal time scales, as well as the multidecadal variability of the NHT in the simulations of the 40 CMIP5 models, which is a much larger ensemble than has been used in previous studies. In addition, based on the work of *Li et al*. [2013], we examine how well the state-of-the-art coupled climate models capture the observed NAO-NHT relationship. The remainder of this paper is organized as follows. Section 2 introduces the data and methods used in this study. An analysis of the performance of the models in reproducing the historical NAO and NHT is presented in section 3. The model simulations of the NAO-NHT relationship are discussed in section 4. Finally, section 5 summarizes our main conclusions and the problems that remain to be solved.

2. Data and Methods

2.1. Data

Observed sea level pressure (SLP) data are obtained from the Hadley Centre's monthly historical mean SLP data set (HadSLP2r) [*Allan and Ansell*, 2006] and the National Center for Atmospheric Research SLP data set (NCAR SLP) [*Trenberth and Paolino*, 1980]. Both SLP data sets have a horizontal resolution of 5° × 5°. SLP from another data set, the National Oceanic and Atmospheric Administration 20th Century Reanalysis Version 2c (20CRv2c) [*Compo et al*., 2011], gives similar results (not shown). The observational surface temperature data set used in this study is version 4 of the combined land and sea surface temperature data set from the UK Met Office Hadley Centre and the Climatic Research Unit at the University of East Anglia (HadCRUT4) [*Morice et al*., 2012], which has a horizontal resolution of 5° × 5°. Observed sea surface temperature (SST) data used in this study are from the Hadley Centre's sea surface temperature data set (HadSST3) [*Kennedy et al*., 2011a, 2011b] in a horizontal resolution of 5° × 5°.

In this study, we analyze simulations from the 40 Atmosphere-Ocean General Circulation Models (AOGCMs) that participated in CMIP5. The model outputs used are based on their availability from the CMIP5 archive (http://cmip-pcmdi.llnl.gov/cmip5), and information related to these models, including their developing centers and horizontal resolutions, is listed in Table 1. To assess the ability of the models to reproduce past climate variability, we use monthly output for the period 1900–2005 from historical simulations that are forced by observed atmospheric composition changes of both natural (e.g., solar irradiance and volcanic aerosols) and anthropogenic (e.g., greenhouse gases, sulfate aerosols, and ozone) sources [*Taylor et al*., 2012]. The results presented in this study are based upon the first realization (r1i1p1) of all models (except EC-EARTH, for which r7i1p1 is used due to data availability) considered. The same analysis of the simulated variability of the NAO and NHT is also completed after concatenating different runs for models that provide ensembles of historical simulations, and the results are generally consistent with those coming from only one realization. As the ocean component of most AOGCMs uses a tripolar global grid, the modeled outputs of ocean variables such as SST are interpolated onto a common rectangular grid of $1° \times 1°$ prior to further calculations.

2.2. Methods

The NAO pattern is defined as the leading empirical orthogonal function (EOF) [*Wilks*, 2006] mode of the SLP field over the North Atlantic region. The EOFs are defined as the eigenvectors of the covariance matrix of the SLP fields. For a regular latitude-longitude grid, the grid points at higher latitudes usually represent a smaller area. To avoid overestimation of the impact of SLPs at higher latitudes, we apply an area-weighting method [*Chung and Nigam*, 1999; *Thompson and Wallace*, 2001; *Handorf and Dethloff*, 2012; *Liu et al*., 2016] to ensure that equal areas are equally weighted. The gridded SLPs are multiplied by the square root of the cosine of their latitude before calculating the EOF modes, so that the covariance matrix is weighted by the cosine of the latitude. To ensure that the NAO patterns are comparable between the different CMIP5 models, we normalize the EOF loading patterns using the standard deviation of the corresponding principal components following the method of *Zheng et al*. [2013] and *Liu et al*. [2016]. Note that, as the NCAR SLP contains missing values in the North Atlantic region during the first half of the twentieth century, we use an alternative method to calculate the NAO pattern for the validation between the two observational data sets. Instead of using the actual EOFs, we first calculate the leading EOF mode for the period without missing values, then calculate the associated principal component (PC) time series for the whole period according to this leading mode, and finally standardize the PC time series and regress the original SLP field of the whole period onto the standardized PC time series to obtain the regressed NAO pattern. We note that other approaches are available, such as using statistical methods to fill the missing points in the SLP data [*Beckers and Rixen*, 2003; *Kondrashov and Ghil*, 2006], which provide an alternative way of validating the observational data sets that could be used in the future. The decadal NAO pattern is defined as the leading EOF mode of the 11 year running average SLP fields over the North Atlantic region. The NAO index (NAOI) is defined as the difference in the normalized SLP, zonally averaged over the North Atlantic sector (80°W–30°E), between the two latitudes that have the strongest negative correlation in SLP variability [*Li and Wang*, 2003; *Li et al*., 2013]. We also examine the NAOI which is defined as the PC of the leading EOF mode. Great consistency is found between these two kinds of NAOIs, with a correlation coefficient of 0.96 (0.97) for HadSLP2r (NCAR SLP) and no less than 0.90 for all of the models. Thus, the results of this study are insensitive to the definition of the NAOI.

The NHT is defined as the mean surface temperature averaged poleward of the equator. The forced component of the NHT variability is estimated by taking the ensemble mean of all CMIP5 simulations based on the assumption that the internal variability can be largely averaged out by taking the ensemble mean of a sufficiently large ensemble. A similar method has been used in previous studies [*Kravtsov and Spannagle*, 2008; *Knight*, 2009; *Knutson et al*., 2013; *Mann et al*., 2014; *Tandon and Kushner*, 2015; *Peings et al*., 2016]. Taking into account the different model sensitivities to the external forcings, estimation of the forced NHT for each model is scaled using the linear regression coefficient of the NHT simulated by each individual model onto the multimodel ensemble mean (MME). Unforced internal variability of the NHT is then obtained by subtracting the estimated forced component of the NHT from the simulated total NHT for each model. The AMO index (AMOI) is defined as the North Atlantic (30°–65°N, 75°W–7.5°E) area-averaged annual mean unforced SST anomalies. When constructing the AMOI, we average the SST anomalies over the North Atlantic domain first and then remove the forced component. The forced component of SST is estimated using the same method as for the determination of the forced variability of the NHT. To avoid contamination by possible model biases in their response to the external forcings, internal variability of the observed NHT time series and AMO is

Table 1. Basic Information of CMIP5 Models Employed in This Study

Name	Modeling Center/Country	Resolution (Latitude × Longitude)	
		Atmosphere	Ocean
ACCESS1-0	Commonwealth Scientific and Industrial Research Organization (CSIRO) and Bureau of Meteorology (BOM)/Australia	145 × 192	300 × 360
ACCESS1-3		145 × 192	300 × 360
BCC-CSM1-1	Beijing Climate Center (BCC), China Meteorological Administration (CMA)/China	64 × 128	232 × 360
BCC-CSM1-1-m		160 × 320	232 × 360
BNU-ESM	College of Global Change and Earth System Science (GCESS), Beijing Normal University (BNU)/China	64 × 128	200 × 360
CanESM2	Canadian Centre for Climate Modelling and Analysis (CCCMA)/Canada	64 × 128	192 × 256
CCSM4	National Center for Atmospheric Research (NCAR)/United States	192 × 288	384 × 320
CESM1-BGC	National Science Foundation (NSF), Department of Energy (DOE), NCAR/United States	192 × 288	384 × 320
CESM1-CAM5		192 × 288	384 × 320
CESM1-FASTCHEM		192 × 288	384 × 320
CESM1-WACCM		96 × 144	384 × 320
CMCC-CESM	Centro Euro-Mediterraneo per I Cambiamenti Climatici (CMCC)/Italy	48 × 96	149 × 182
CMCC-CM		240 × 480	149 × 182
CMCC-CMS		96 × 192	149 × 182
CNRM-CM5	Centre National de Recherches Meteorologiques (CNRM) and Centre Europeen de Recherche et Formation Avancees en Calcul Scientifique (CERFACS)/France	128 × 256	292 × 362
CSIRO-Mk3-6-0	CSIRO with Queensland Climate Change Centre of Excellence (QCCCE)/Australia	96 × 192	189 × 192
EC-EARTH	EC-EARTH consortium/Various	160 × 320	292 × 362
FGOALS-g2	National Aeronautics and Space Administration (LASG), Institute of Atmospheric Physics (IAP), Chinese Academy of Sciences (CAS)/China	60 × 128	196 × 360
FGOALS-s2		108 × 128	196 × 360
GFDL-CM3	National Aeronautics and Space Administration (NOAA) Geophysical Fluid Dynamics Laboratory (GFDL)/United States	90 × 144	200 × 360
GFDL-ESM2G		90 × 144	210 × 360
GFDL-ESM2M		90 × 144	200 × 360
GISS-E2-H	National Aeronautics and Space Administration (NASA) Goddard Institute for Space Studies (GISS)/United States	90 × 144	90 × 144
GISS-E2-R		90 × 144	90 × 144
HadCM3	Met Office Hadley Centre (MOHC; additional HadGEM2-ES realizations contributed by Instituto Nacional de Pesquisas Espaciais)/United Kingdom	73 × 96	144 × 288
HadGEM2-ES		145 × 192	216 × 360
INM-CM4	Institute for Numerical Mathematics (INM)/Russia	120 × 180	340 × 360
IPSL-CM5A-LR	Institut Pierre-Simon Laplace (IPSL)/France	96 × 96	149 × 182
IPSL-CM5A-MR		143 × 144	149 × 182
IPSL-CM5B-LR		96 × 96	149 × 182
MIROC-ESM	Japan Agency for Marine-Earth Science and Technology (JAMSTEC), Atmosphere and Ocean Research Institute (AORI; The University of Tokyo), and National Institute for Environmental Studies (NIES)/Japan	64 × 128	192 × 256
MIROC-ESM-CHEM		64 × 128	192 × 256
MIROC5		128 × 256	224 × 256
MPI-ESM-LR	Max Planck Institute for Meteorology (MPI-M)/Germany	96 × 192	220 × 256
MPI-ESM-MR		96 × 192	404 × 802
MPI-ESM-P		96 × 192	220 × 256
MRI-CGCM3	Meteorological Research Institute (MRI)/Japan	160 × 320	368 × 360
MRI-ESM1		160 × 320	368 × 360
NorESM1-M	Norwegian Climate Centre (NCC)/Norway	96 × 144	384 × 320
NorESM1-ME		96 × 144	384 × 320

obtained by simply removing the linear trend. Estimating the unforced component by removing the MME from the observed NHT and AMO does not make significant change to our results. The Atlantic meridional overturning circulation (AMOC) index (AMOCI) is defined as the maximum AMOC stream function at 40°N and below 500 m.

All of the anomalies for the climate variables are calculated relative to the reference period of 1961–1990. The statistical significance of the correlation between the two auto-correlated time series is examined using a two-tailed Student's *t* test with an effective number of degrees of freedom N^{eff}. The value of N^{eff} is given by the following approximation [*Pyper and Peterman*, 1998; *Li et al*., 2013; *Sun et al*., 2015a, 2015b; *Xie et al*., 2016]:

$$\frac{1}{N^{\text{eff}}} \approx \frac{1}{N} + \frac{2}{N}\sum_{j=1}^{N}\frac{N-j}{N}\rho_{XX}(j)\rho_{YY}(j),$$

where N is the sample size, and $\rho_{XX}(j)$ and $\rho_{YY}(j)$ are the autocorrelations of the two sampled time series X and Y at time lag j.

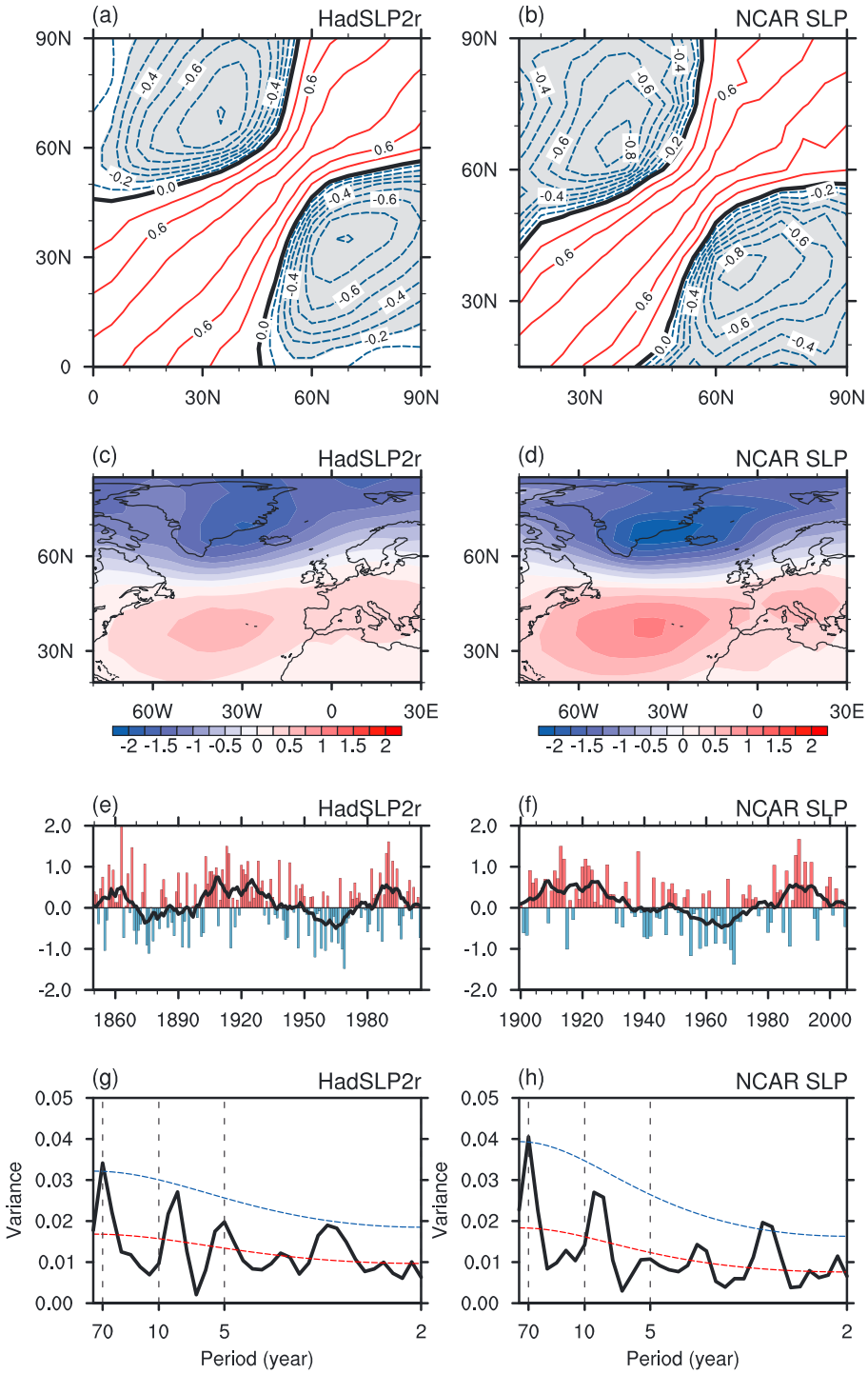

Figure 1. Observed spatial and temporal characteristics of the NAO derived from (left column) HadSLP2r and (right column) NCAR SLP. (a, b) Cross-correlation coefficients between regionally zonal-averaged annual mean SLPs over the North Atlantic region (80°W–30°E) for the period 1900–2005. The red solid (blue dashed) contours represent positive (negative) values at an interval of 0.3 (0.1), and the significant negative correlations at the 95% confidence level are shaded. (c, d) Spatial pattern of the NAO displayed as the regression map of the annual mean sea level pressure (SLP) onto their standardized PC time series of 1900–2005. Time series of the NAOI for the period (e) 1850–2005 and (f) 1900–2005. The thick black curve indicates 11 year running means. Power spectrum of the annual mean NAOI for the period (g) 1850–2005 and (h) 1900–2005. The blue and red dashed lines show the 95% confidence level and the reference red noise spectrum, respectively.

3. Performance of CMIP5 Models in Reproducing the NAO and NHT

3.1. Observed Spatial and Temporal Characteristics of the NAO

Figure 1 displays the observed spatial and temporal features of the NAO determined from the HadSLP2r and NCAR SLP data. The cross correlations between regional (80°W–30°E) zonal-averaged SLPs show statistically significant negative correlations between the middle and high latitudes (Figures 1a and 1b), indicating that the NAO reflects a north-south seesaw in atmospheric mass over the North Atlantic sector [*Li and Wang*, 2003]. In accordance with the cross correlations, the NAO patterns derived from our EOF analysis show out-of-phase changes between the Icelandic Low and Azores High (Figures 1c and 1d). The positive phase of the NAO features higher (lower) pressures at middle (high) latitudes. There is great consistency between the two data sets in the spatial pattern of the NAO, with a pattern correlation of 0.98.

Figures 1e and 1f display the annual mean NAOI calculated using the definition of *Li and Wang* [2003], and the NAO time series shows variations over multidecadal, as well as interannual, time scales. This feature can be clearly demonstrated using continuous power spectrum analysis (Figures 1g and 1h). The observed NAOI shows a significant spectral peak with a period of approximately 70 years. In addition, there are obvious peaks over quasi-decadal scales of around 8 years and interannual scales of about 2.7 years. Similarly, the previous literature concerning the temporal behavior of the winter mean NAO also reports enhanced spectral power over quasi-decadal (~8 years) and interannual (2–3 years) time scales [*Hurrell and Van Loon*, 1997; *Cook et al*., 1998; *Wunsch*, 1999; *Marshall et al*., 2001; *Gámiz-Fortis et al*., 2002; *Hurrell et al*., 2003]. It must be pointed out that the statistical significance of the multidecadal variation should be interpreted carefully, as the analysis period covers only two cycles for HadSLP2r and one and a half cycles for NCAR SLP. Nevertheless, a multidecadal oscillation of 50–70 years was found in several studies based on reconstructed NAO time series [*Cook et al*., 1998; *Wanner et al*., 2001; *Mazzarella and Scafetta*, 2012; *Olsen et al*., 2012]. *Sun et al*. [2015b] identified a quasi 60 year oscillation in both reconstructed data and model simulations and proposed a delayed oscillator model to explain the mechanism associated with the NAO's quasiperiodic multidecadal variability, which is a result of the air-sea interaction and slow oceanic processes over the North Atlantic region. Besides, the 60–70 year fluctuation is also found in global and regional temperatures [*Schlesinger and Ramankutty*, 1994; *Delworth and Mann*, 2000]. As with the spatial characteristics, the temporal variations of the NAO determined from the two data sets are highly consistent.

In the following section, the CMIP5 model simulations of the NAO variability will be systematically analyzed from both the spatial and temporal viewpoints. The simulations and observations are compared to examine the ability of the CMIP5 models to reproduce historical NAO variability. As some values are missing from the NCAR SLP data set, we use mainly the HadSLP2r data for the model validation.

3.2. Model Simulated NAO Variability

The cross correlation of the regional zonal-averaged SLPs over the North Atlantic sector simulated by the CMIP5 models (Figure A1) shows that all models can reproduce the seesaw structure of the NAO reasonably well, with significant negative correlations between middle and high latitudes. The maximum negative correlation varies from −0.61 (CESM1-WACCM) to −0.86 (GFDL-CM3; Figure 2b). Compared with the observational value of −0.81 (−0.84) for HadSLP2r (NCAR SLP), the CMIP5 models tend to underestimate the circulation variability associated with the NAO. The latitudinal positions of the two centers of action of the NAO are measured as the latitudes at which the zonally averaged SLPs have the strongest negative correlation. In observations, the two centers of action are located at 35°N and 65°N for NCAR SLP and 35°N and 70°N for HadSLP2r. Note that both data sets have a horizontal resolution of 5° × 5°, and the correlation between regional zonal-averaged SLPs for HadSLP2r at 35°N and 65°N is −0.80, which is nearly the same as that between 35°N and 70°N. Besides, the latitudes of the centers of action reported by *Li and Wang* [2003] are also around 35°N and 65°N. Thus, to a large extent, the inconsistency between the two data sets can be ascribed to grid definition. To prevent any possible influence of interpolation on the result, we use uninterpolated grid data from each model in this calculation. As shown in Figure 2a, there is a spread of approximately 10° for both centers of action. The simulated latitudes of the Icelandic Low range from 62.79°N (FGOALS-g2) to 73.46°N (EC-EARTH), with most distributed around 65°–70°N. Concerning the Azores High, the southernmost locations are at 33°N (GISS-E2-R) and the northernmost location reaches 46.42°N (NorESM1-M). Most are located within a band about 5° wide centered on 40°N. When compared with the observational data, most of the simulated latitudes of the Azores High and the Icelandic Low are displaced to the north. Nevertheless, the models

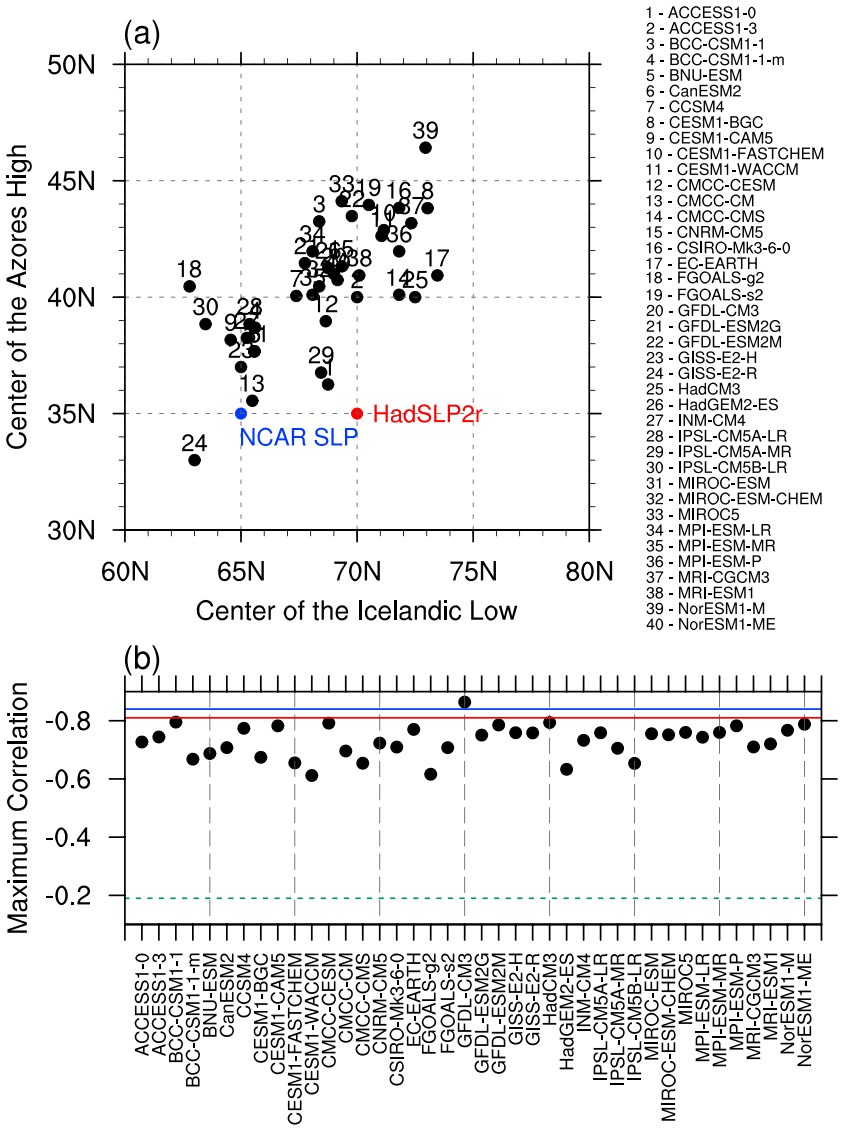

Figure 2. (a) Latitudinal locations of the two centers of action of the NAO. Numbered black dots represent the 40 CMIP5 models whose names are listed on the right. The red (blue) dot refers to the observed result from HadSLP2r (NCAR SLP). Vertical and horizontal axes indicate the latitudes of the center of Azores High and Icelandic Low, respectively. (b) Maximum negative correlation coefficients of regionally zonal-averaged SLPs between middle and high latitudes obtained from CMIP5 model simulations (black dots), HadSLP2r (red line), and NCAR SLP (blue line). The green dashed line indicates the 95% confidence level.

generally agree well with the observations in the latitudinal distance between the two centers of action, which is about 30°.

The leading EOF mode of the simulated annual mean SLPs over the North Atlantic region is calculated for each model as well as for HadSLP2r to further examine the performance of the models in reproducing the spatial pattern of the NAO. Figures 3a and 3c display the interannual EOF pattern derived from HadSLP2r, and the MME of the historical runs, respectively. It can be seen that the models considered in this study are able to reasonably reproduce the dipole structure of the leading mode of the North Atlantic SLP field. In the observations, the NAO explains 45.6% of the SLP variability over the North Atlantic region. The estimated margin of error of this percentage is 6.3% according to the method detailed by *North et al.* [1982]. In the model simulations, the explained variances range from 33.0% (HadGEM2-ES) to 54.5% (CMCC-CESM). Taking into account the range of uncertainty, most models give a reasonable simulation of the explained variance of the NAO.

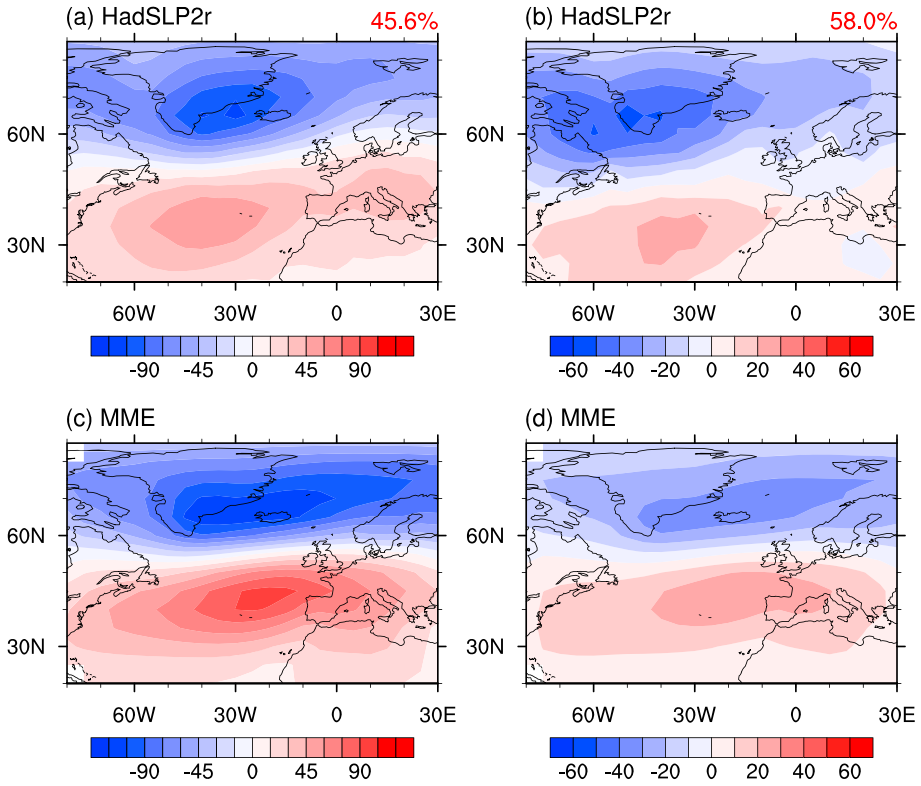

Figure 3. Leading EOF mode of the (a) annual mean and (b) decadally smoothed SLP field over the North Atlantic region derived from HadSLP2r. The red numbers at the top right corner indicate the explained variance. (c and d) as in Figures 3a and 3b but for the MME of CMIP5 historical simulations.

We use a Taylor diagram [*Taylor*, 2001] to quantitatively measure the difference between model simulations and observations and to make intuitive comparisons among the different models. Figure 4a shows that almost all of the pattern correlation coefficients between the modeled and observed interannual NAO patterns are no less than 0.90, indicating that the CMIP5 models generally give a good representation of the NAO pattern. Despite the difference in the definition of the NAO pattern and the period of study, these coefficients are generally higher than those obtained previously using the CMIP3 models [*Casado and Pastor*, 2012; *Handorf and Dethloff*, 2012], indicating that the CMIP5 models improve the simulation of the NAO's spatial pattern. Nevertheless, compared with the observations, the model results show some biases with respect to the location and amplitude of the pressure centers.

The latitudinal locations of the two centers of action of the NAO simulated by individual models (Figure A2) are consistent with the result obtained from the cross-correlation analysis of the SLPs. That is, most of the simulated Azores Highs are situated to the north of its observed location. For longitudinal locations, nearly half of the simulated Icelandic Lows, and almost all of the simulated Azores Highs, have an eastward displacement when compared with the observations. On the other hand, as shown in the Taylor diagram (Figure 4a), the ratios of the standard deviations between modeled and observed NAO patterns spread from about 1.11 (CESM1-WCCM and FGOALS-g2) to 1.92 (CMCC-CESM). All models reproduce a larger range of annual mean SLP anomalies over the North Atlantic domain than seen in HadSLP2r. In general, GISS-E2-H, ACCESS1-0, and GISS-E2-R perform best at reproducing the interannual NAO pattern.

We next assess the ability of the CMIP5 models to handle the temporal behavior of the NAO from several different standpoints, including the Taylor diagram and power spectrum analysis. A pair of Taylor diagrams is used to quantify the similarity between the simulated and observed annual mean (Figure 5a), as well as decadal (Figure 5b), NAOI. Note that the NAO is driven mainly by internal atmospheric dynamics, and historical simulations are initiated from an arbitrary point in a quasi-equilibrium control run [*Taylor et al.*, 2012]. Therefore, the modeled evolution of the NAO time series cannot be expected to exactly coincide with

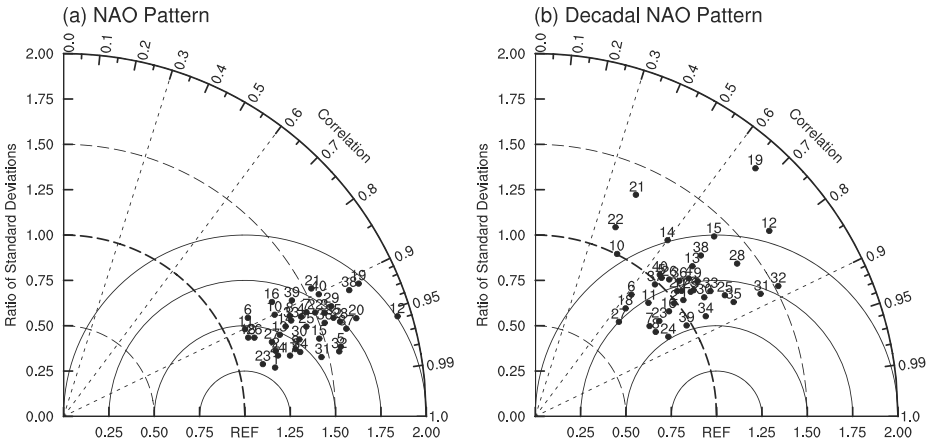

Figure 4. Taylor diagram of the (a) NAO pattern and (b) decadal NAO pattern. Each numbered dot in the diagram represents a single model (see Figure 2a for which model each number represents). The term "REF" on the horizontal axis refers to the reference point. Black dashed lines and arcs indicate the correlation coefficient and the ratio of standard deviations between modeled and observed (HadSLP2r) NAO patterns, respectively. Black solid arcs show the centered root mean square difference which is equal to the radical distance from the reference point.

either the observations or the evolutions simulated by other models. The large spread of the coefficients indicates the differences among the models with respect to the interpretation of internal climatic variability. The ratios of the standard deviations between the modeled and observed annual mean NAOI are generally close to 1.0, showing that the models performed well in reproducing the amplitude of the interannual variability of the NAO. However, for the decadal NAOI, all of the ratios, except for FGOALS-s2, are less than 1.0. Apparently, for decadal and longer time scales, most CMIP5 models underestimate the amplitude of the NAO.

Another important aspect of the temporal behavior of the NAO is its spectral characteristics. Here we use the continuous power spectrum to examine the performance of the CMIP5 models in reproducing the spectral structure of the NAO. We find a considerable difference in the distribution of spectral power among the models (Figure 6a). The spectrum of the observed NAO series is slightly red, which means greater spectral power at lower frequencies. However, this is not seen in most model simulations. Spectral power over multidecadal time scales is underestimated by almost all of the models except FGOALS-s2. This is consistent with the above result that only this model simulates a larger standard deviation of the decadal NAOI than seen in the observations. As summarized in Figure 6b, the observed spectral peak at 2–3 years is captured by 16 of the models, and the enhanced energy at around 8 years is generated by only eight models. Based on their studies using the CMIP3 models, *Handorf and Dethloff* [2012] also reported the lack of a quasi-decadal spectral peak in most of the model simulations. When focusing on the multidecadal scale, only seven models (FGOALS-s2, GFDL-ESM2G, GISS-E2-R, HadGEM2-ES, IPSL-CM5A-LR, MIROC-ESM, and MIROC5) show enhanced energy over multidecadal time scales, but this was not statistically significant. Taken together, only a minority of the CMIP5 models reproduce the classical spectral peaks of the NAOI, whereas most models tend to underestimate the spectral power over the decadal to multidecadal scales.

Although reproduction of the observed temporal evolution of the decadal NAOI by the CMIP5 models cannot be expected, a few models do indeed show enhanced spectral power over decadal and multidecadal scales. Therefore, it is necessary to further explore how well the NAO pattern of decadal to multidecadal time scales is simulated. Figure 3b shows the decadal pattern of the NAO derived from the HadSLP2r data. The decadal EOF pattern is obtained by performing EOF analysis on the SLP fields smoothed using an 11 year running mean. In the observations, the NAO is the leading EOF mode and explains 58.0%, with a margin of error of 8.0%, of the decadal variability over the North Atlantic area. Compared with the interannual NAO pattern, the amplitude of the decadal NAO pattern is smaller. However, the decadal dipole pattern is only slightly different from the interannual pattern, with a westward shift of the Icelandic Low and a southward shift of the Azores High. Similarly, *Woollings et al.* [2015] distinguished SLP patterns associated with the NAO variabilities over multidecadal and interannual-decadal time scales and found that there are only subtle differences between them.

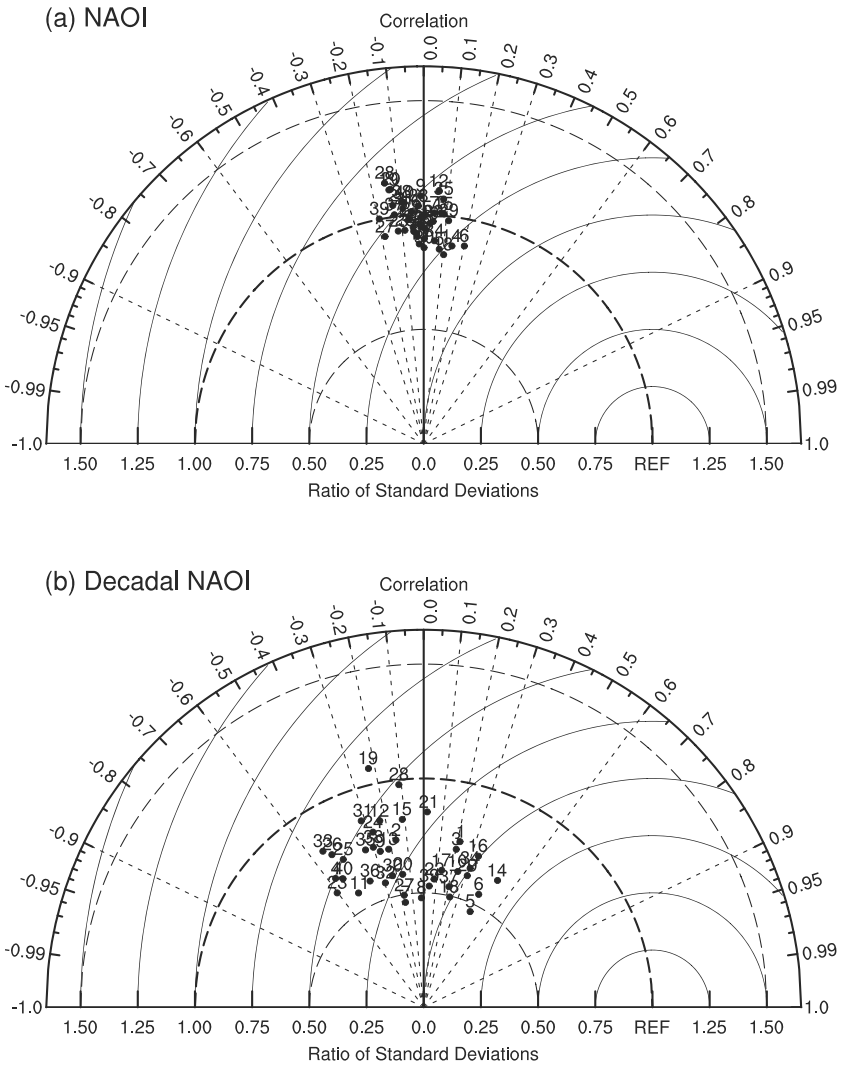

Figure 5. Taylor diagram of the (a) annual mean and (b) 11 year running-averaged NAOI. See Figure 2a for which model each number represents.

Generally, compared with the interannual NAO pattern, larger inconsistencies with respect to the observations are evident in the simulated decadal NAO pattern (Figure A3). The correlation between the simulated and observed decadal NAO patterns is no greater than 0.90 for any of the models (Figure 4b). The MME pattern (Figure 3d) shows a clearly eastward displacement for both centers of action of the decadal NAO when compared with the observations (Figure 3b). In addition, most of the simulated Azores Highs are located north of the observed location. There is a large spread in the ratios of the standard deviations of the simulated and observed decadal NAO patterns among the models (Figure 4b). Most of the ratios are larger than 1.0, although the MME pattern shows a smaller maximum in the centers of action of the NAO (Figure 3d). This is probably due to the fact that the decadal NAO pattern in the models is more spread out over the domain, which leads to higher spatial standard deviation despite smaller maxima in the centers of action.

In most of the model simulations, the NAO is the first EOF mode of decadal SLP variability over the North Atlantic sector. However, for INM-CM4, the first mode shows a tripole pattern (not shown), and the second mode is closer to the NAO. In fact, the first two EOF modes simulated by INM-CM4 are not independent of each other based on the criterion suggested by *North et al*. [1982]. The explained variance of the decadal NAO mode varies considerably among the models. For example, the smallest and largest variances are 34.4% (FGOALS-g2) and 72.7% (FGOALS-s2), respectively. Taking the uncertainty of this value into account,

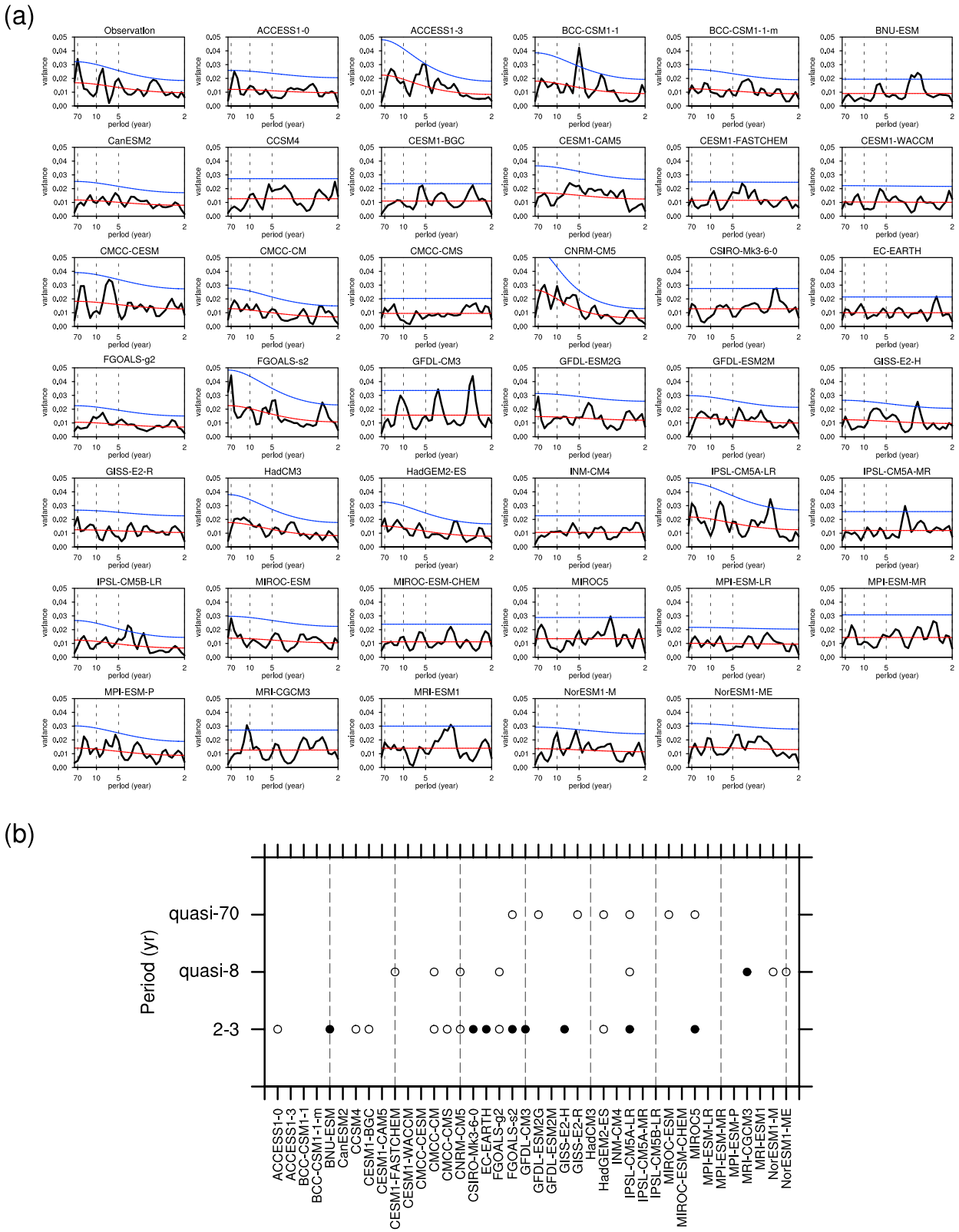

Figure 6. (a) Power spectrum of the NAOI derived from HadSLP2r as well as individual CMIP5 models. The blue and red dashed lines show the 95% confidence level and the reference red or white noise spectrum, respectively. (b) Summary of the performance of CMIP5 models in reproducing NAO's spectral structure. A solid dot indicates that the model simulates a significant peak at the 95% confidence level. A circle indicates that the simulated spectrum shows enhanced power for the considered period though not statistically significant.

more than half of the models underestimate the variance explained by the decadal NAO. Models that show enhanced energy over multidecadal scales in the power spectrum analysis generally have larger explained variances of the decadal variability in the North Atlantic SLP field than do the other models.

Recent work has shown that internally generated climate variability could induce large differences in the simulated NAO variability across different ensemble members in the same model [*Deser et al*., 2016]. This kind of sampling variability should be taken into consideration when evaluating model performance. We use a method similar to that introduced by *Deser et al*. [2016] to estimate the uncertainty in the simulated NAO pattern. The range of error at each grid point of the simulated EOF pattern is measured as the doubled standard deviation of the values generated by all ensemble members at that point. As it provides 10 historical runs, which is the largest ensemble among the models considered in this study, we use the simulations from CNRM-CM5 as an example. We found that internal stochastic variability can induce a sampling error of about ±18 Pa in the simulated amplitude of the interannual NAO pattern. With respect to the decadal NAO pattern, the range of error is about ±12 Pa for the Icelandic Low and ±20 Pa for the Azores High, which indicates a much larger uncertainty because the amplitude of the decadal NAO pattern is relatively smaller. Thus, longer simulations may be needed to better analyze the simulated NAO characteristics over decadal time scales. As it is not easy to estimate the sampling error of an EOF pattern, and we have made just a simple attempt here, further effort will be needed to allow more thorough analysis in the future.

3.3. Model Simulation of the Multidecadal NHT

The variation of the NHT is a combination of internal unforced variability as well as a response to external forcings from both natural and anthropogenic sources. The general features of the historical NHT evolution that reflects both internal and forced variabilities are reproduced reasonably well by coupled climate models [*Zhou and Yu*, 2006; *Flato et al*., 2013; *Jones et al*., 2013; *Knutson et al*., 2013]. As shown in Figure 7a, the decadally smoothed NHT anomalies that incorporate both unforced and forced components simulated by the CMIP5 models are generally highly correlated with the observations (HadCRUT4). Most of the correlations are greater than 0.90, and almost all of them are greater than 0.80. More than half of the ratios of the standard deviations between modeled and observed decadal NHT anomalies fall within the range 0.75 to 1.25. This indicates that, consistent with earlier studies [*Flato et al*., 2013; *Jones et al*., 2013; *Knutson et al*., 2013], most CMIP5 models can acceptably reproduce the temporal evolution, as well as the amplitude, of the multidecadal NHT when the forced and internal variabilities are not separated.

How well do the CMIP5 models reproduce the internal variability of the multidecadal NHT? We use the methods described in section 2 to estimate the internal variabilities of the modeled and observed NHT anomalies and make a comparison between them. Figure 7b shows the Taylor diagram of the internal-only variability of the decadally smoothed NHT anomalies. As an internally generated variability, the temporal evolution of the unforced NHT in model simulations cannot be expected to synchronize with the observations, and the relatively low correlations in Figure 7b demonstrate this. The simulated amplitudes of the internal decadal NHT anomalies vary markedly among the models. For example, the ratio of standard deviations to the observations is 1.27 for HadGEM2-ES but only 0.32 for GISS-E2-R. Generally, most models underestimate the decadal fluctuation of the internal NHT anomalies.

In summary, although the CMIP5 models reproduce the multidecadal variability of the historical NHT reasonably well, they tend to underestimate the internal part of the multidecadal NHT. This indicates that the CMIP5 historical simulations of the NHT may be overly influenced by external forcings, and the success of the models in reproducing the historical NHT variability is largely dependent on their accurate interpretation of the forced component of the NHT. Previous studies reported that internal climate modes such as the Interdecadal Pacific Oscillation (IPO) [*Dai et al*., 2015; *Kosaka and Xie*, 2016] and El Niño–Southern Oscillation (ENSO) [*Schmidt et al*., 2014] may contribute to the stimulation of the internal variability of the global mean surface temperature. However, less attention has been paid to the contribution of the NAO. Based on observational and theoretical modeling analysis, *Li et al*. [2013] found that the NAO is an important driver of the NHT multidecadal variability, and about two thirds of the variance of the multidecadal NHT can be explained as a response to this NAO variability. Furthermore, *Keenlyside et al*. [2008] suggested the importance of the NAO's role in the decadal prediction of global temperature. These studies provide some indication of why the models tend to underestimate the multidecadal internal variability of the NHT. Our analysis in section 3.2 suggests that the CMIP5 models tend to underestimate the observed decadal to multidecadal

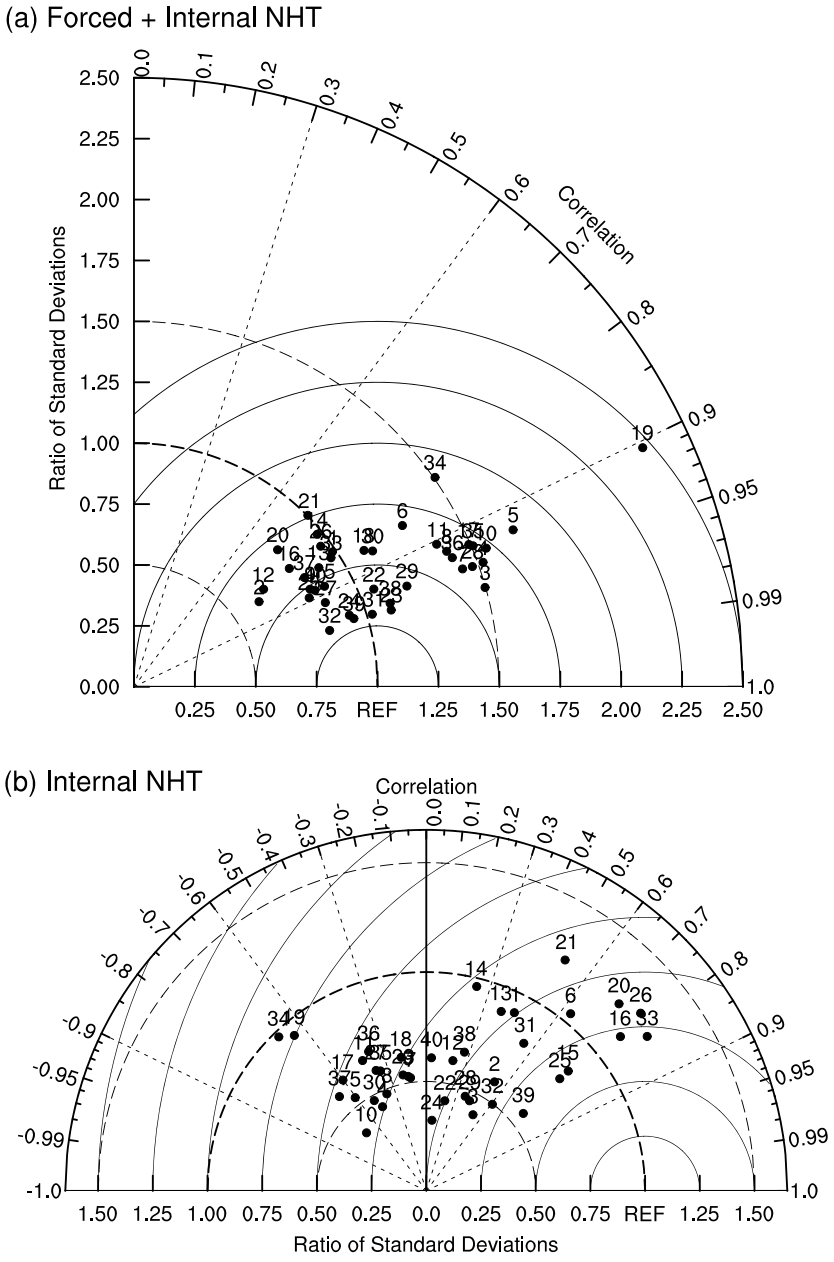

Figure 7. Taylor diagram of the decadal NHT anomalies for (a) forced and internal variabilities and (b) internal variabilities only. See Figure 2a for which model each number represents.

variability of the NAO. This may be one of the possible reasons for their underestimation of the internal variability of the NHT. In the following section, we will explore the representation of the NAO-NHT relationship in the CMIP5 models.

4. NAO-NHT Relationship in Model Simulations

Li et al. [2013] identified a significant phase lag between the observed NAO and NHT. The correlation coefficients are positive when the NAO leads the detrended NHT by 10–20 years and reaches a maximum when the NAO leads by 16 years. Based on their study, we further examine whether the CMIP5 models can reproduce this relationship. Figure 8 displays the simulated lead-lag correlations between the NAO and internal NHT anomalies time series based on the annual mean, as well as decadally smoothed data covering the period

1900–2005. One well-defined feature is that the lead-lag correlations for the 40 models show highly varying patterns. Qualitatively, there are 11 models (ACCESS1-0, BCC-CSM1-1-m, CCSM4, CESM1-CAM5, CSIRO-Mk3-6-0, INM-CM4, IPSL-CM5A-LR, MIROC-ESM, MIROC-ESM-CHEM, MPI-ESM-MR, and NorESM1-ME) that reproduce a significant positive correlation when the NAO leads the NHT by more than 5 years. Another three models (CanESM2, CMCC-CMS, and GFDL-ESM2G) also reproduce a decadal lead of the NAO, but this is not statistically significant. In addition, for BCC-CSM1-1, CESM1-BGC, CMCC-CM, and CNRM-CM5, there is a nearly in-phase decadal fluctuation between the NAO and the internal NHT. Discrepancies in the modeled lead-lag correlations between the NAO and the internal NHT are possibly caused by the differences in how the various models represent the physical processes that contribute to the NAO-NHT relationship.

In fact, the physical mechanism associated with the multidecadal variability over the North Atlantic sector has been discussed in many previous studies. Modeling studies show that the forcing effect related to the NAO may contribute to the multidecadal variation of the AMOC, which then influences the meridional heat transport that can further cause the SST signatures of the AMO [*Delworth and Greatbatch*, 2000; *Eden and Jung*, 2001; *Latif et al*., 2006a, 2006b; *Park and Latif*, 2010; *Sun et al*., 2015b]. The warming or cooling effect of the AMO will simultaneously impact the surface temperature over the NH [*Sutton and Hodson*, 2005; *Knight et al*., 2005; *Zhang et al*., 2007; *Wyatt et al*., 2012]. Thus, the AMO may act as a pathway for allowing a delayed influence of the NAO onto the NHT [*Li et al*., 2013; *Sun et al*., 2015b].

Significant positive correlations when the NAO leads the AMO by approximately 15–20 years have been found in both observational [*Li et al*., 2013] and model [*Sun et al*., 2015b] studies, reflecting the delayed oceanic response to the atmospheric forcing mentioned in the last paragraph. Here we also calculate the lead-lag correlations between the NAO and AMO indices for each individual model to examine whether this relationship can be captured by the CMIP5 models. About half of the models agree on the NAO's lead of the AMO in the historical simulations, although the lead time differs among models (Figure A4). Similarly, consensus regarding a 5 year lead of the NAO over the AMO is also reported by *Peings et al*. [2016] based on analysis of the preindustrial control runs [*Taylor et al*., 2012] of the CMIP5 models. In addition, for all models that roughly capture the NAO-NHT phase lag, except CCSM4, a positive correlation is evident when the AMO is led by the NAO. In addition, the simulated lag time is consistent with that between the NAO and the internal NHT. This means that the strengthening of the NAO is followed by a positive phase of the AMO after several years to a decade, and warming over the North Atlantic region will simultaneously heat the entire NH. We note that some models, such as ACCESS1-3, CESM1-BGC, CMCC-CESM, HadGEM2-ES, and MRI-CGCM3, give a positive correlation when the NAO leads the AMO by around a decade but fail to catch the phase lag between the NAO and NHT. This may be because the NHT variability is not induced by AMO heating alone, meaning that the NHT variability seen in these models may be dominated by other factors.

Among the 40 models studied here, the AMOC output from 10 (CNRM-CM5, FGOALS-g2, GISS-E2-R, MIROC5, MPI-ESM-LR, MPI-ESM-MR, MPI-ESM-P, MRI-ESM1, NorESM1-M, and NorESM1-ME) is available, which allows us to further explore the discrepancies in the simulated NAO-NHT connection among these models. We divided these 10 models into two categories, based on whether they can reproduce the NAO's lead on the NHT. Category I contains two models, MPI-ESM-MR and NorESM1-ME, which portray significant positive correlations when the NHT is led by the NAO. The other eight models (CNRM-CM5, FGOALS-g2, GISS-E2-R, MIROC5, MPI-ESM-LR, MPI-ESM-P, MRI-ESM1, and NorESM1-M), which are not able to capture the significant phase lag between the NAO and the NHT, are classified as Category II.

To examine the possible contribution of the AMOC to the NAO-NHT connection, we calculated the lead-lag correlations between the NAOI and AMOCI for each Category I model. In Figure 9a, a positive correlation peak can be seen when the decadal NAOI leads the AMOCI by about 9 years for MPI-ESM-MR and 2 years for NorESM1-ME. The maps of the lagged correlation between the NAO and the AMOC stream function (Figures 9c and 9e) show positive correlations spreading over the North Atlantic Ocean. This indicates that the AMOC tends to strengthen several years after the NAO turns to its positive phase. The difference in the lead-time of the NAO over the AMOC indicates the difference in the response time of the ocean to the NAO forcing simulated by the different models. On the other hand, the AMOC varies nearly in phase with the AMO (Figure 9b) for the Category I models, and the lagged correlation maps between the AMOCI and SST over the North Atlantic region (SST lags the AMOCI by 0 years for MPI-ESM-MR and 4 years for NorESM1-ME) show a homogeneous pattern that resembles the AMO signature (Figures 9d and 9f). This

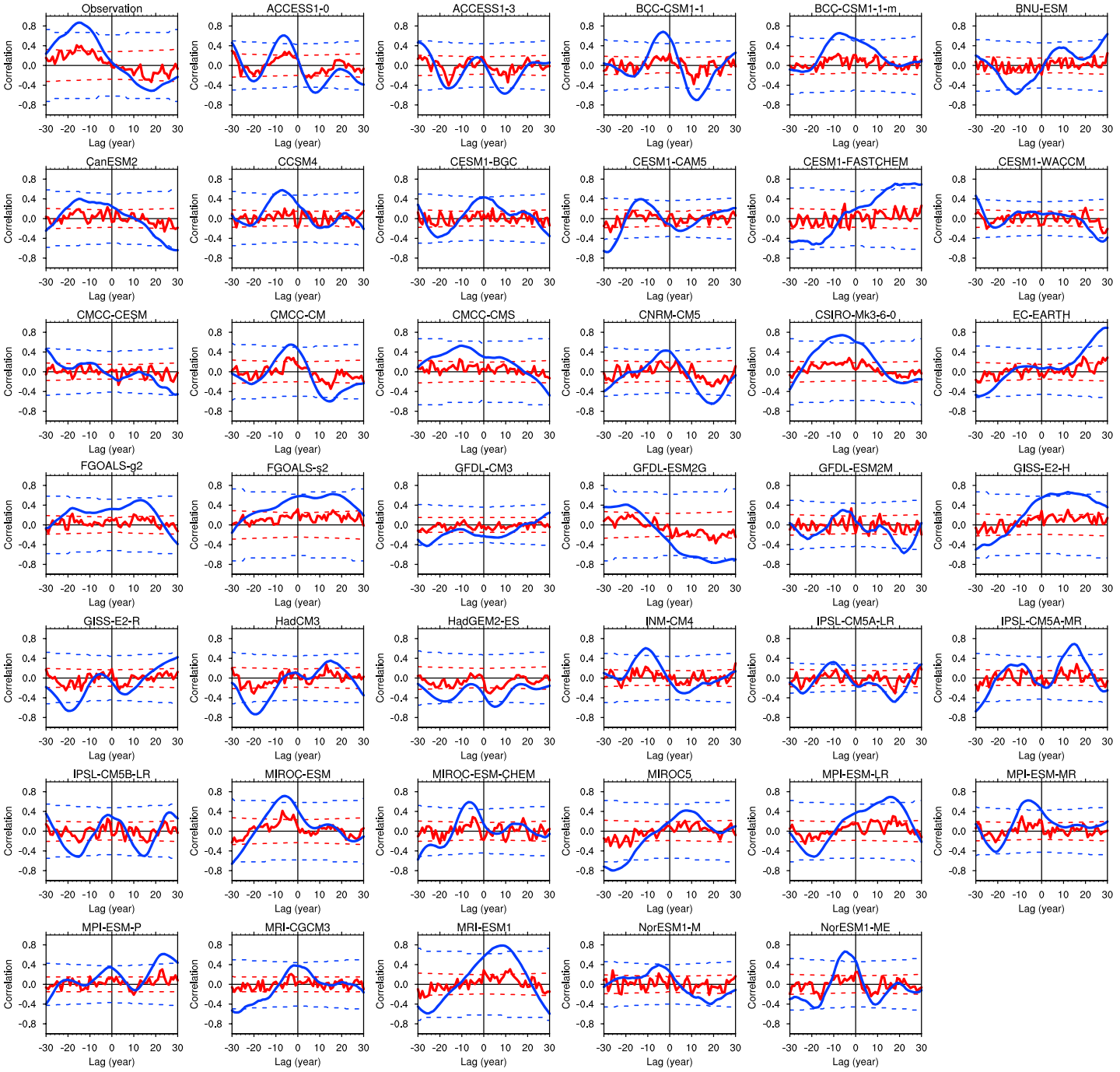

Figure 8. Lead-lag correlation coefficients between the NAOI and internal NHT anomalies derived from the observations as well as CMIP5 historical simulations. The red (blue) curve is for the annual mean (11 year running-averaged) time series. Negative (positive) lag means that the NAO is leading (lagging). The red (blue) dashed curves indicate the 90% confidence level for the unsmoothed (smoothed) time series determined using the effective number of degrees of freedom.

indicates that the strengthened AMOC will lead to the warming of the North Atlantic SST, possibly through the heat convergence induced by the enhanced meridional heat transport. Therefore, the physical processes underlying the delayed response of the AMO to the NAO reported in previous studies [*Eden and Jung*, 2001; *Latif et al.*, 2006a, 2006b; *Park and Latif*, 2010; *Sun et al.*, 2015b] is reproduced by the Category I models. These common features of the Category I models can be seen clearly in the MME curve (Figures 9a and 9b).

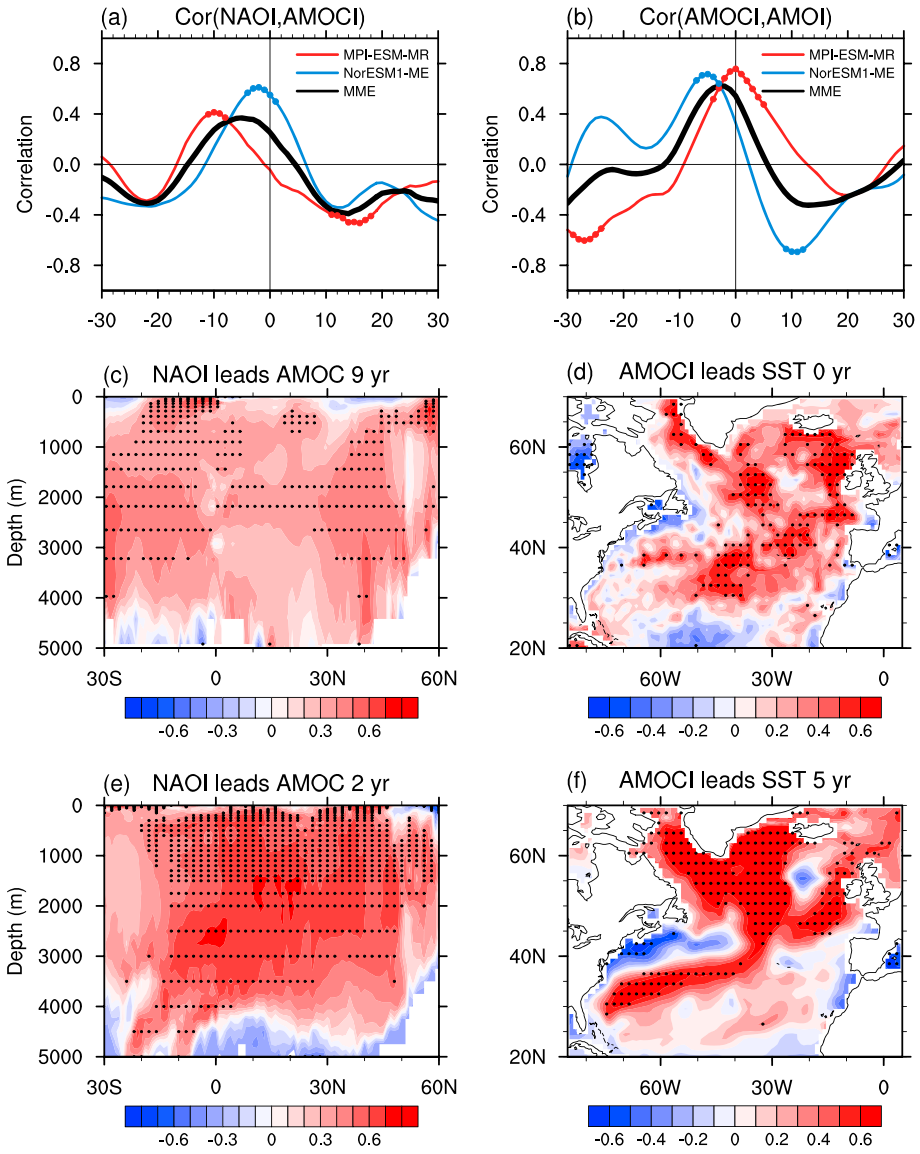

Figure 9. (a) Lead-lag correlations between the decadally smoothed NAOI and AMOCI for each model from Category I as well as the MME. Negative (positive) lag means that the NAOI is leading (lagging). Dots on the curves indicate that the correlations are significant at the 90% confidence level. (b) As in Figure 9a but for the lead-lag correlations between the decadally smoothed AMOCI and AMOI. Negative (positive) lag means that the AMOCI is leading (lagging). The term Cor (*x*, *y*) in Figures 9a and 9b denotes the correlation analysis between the variables *x* and *y*. (c) Lagged correlation map between the decadally smoothed NAOI and AMOC stream function for MPI-ESM-MR. (d) Lagged correlation map between the decadally smoothed AMOCI and SST over the North Atlantic region for MPI-ESM-MR. (e and f) as in Figures 9c and 9d but for the results of NorESM1-ME. Dots in Figures 9c–9f indicate that the correlations are significant at the 90% confidence level.

In contrast, for the Category II models, although most models agree with a lead of around 0–10 years in the fluctuation of the AMOC relative to the AMO (Figure 10b), the strengthening of the AMOC several years after the positive NAO forcing reproduced by the Category I models is not captured by the Category II models (Figure 10a). Some of the Category II models present a weakened AMOC after the positive phase of the NAO. The MME of the NAO-AMOC correlations for the Category II models are weak at all considered lags. Possibly because of the absence of this oceanic response process, we found no significant positive correlations between the NAO and the AMO of subsequent years for the Category II models (Figure A4). This is a possible explanation for the absence of the NAO-NHT relationship in the Category II model simulations. Therefore, capturing the ocean processes related to the AMOC may play an important role in the successful simulation of the observed NAO-NHT connection.

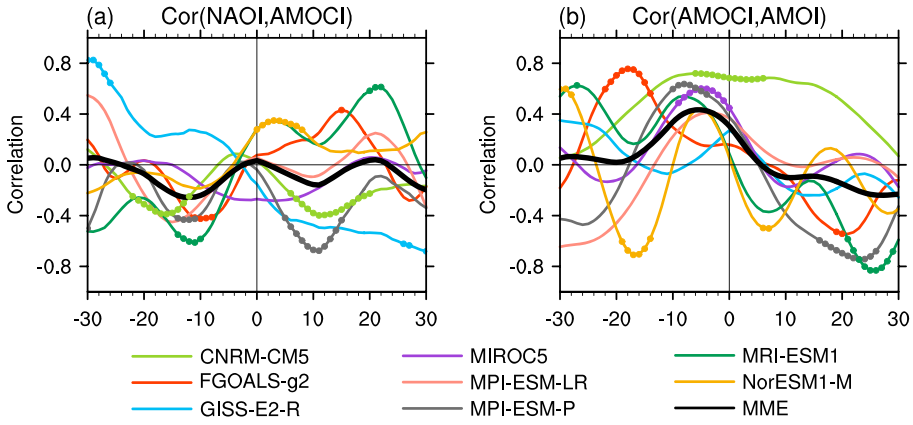

Figure 10. As in Figures 9a and 9b but for the result of Category II models.

The main findings in this section are summarized in Figure 11. It can be seen clearly that all of the models that reproduce the leading influence of the NAO on the NHT, except CCSM4, also capture its influence on the AMO as well as the AMOC (when available). Therefore, the ability of CMIP5 models in reproducing the observed NAO-NHT relationship is possibly related to their performance in simulating the underlying physical processes involved with the AMO and the AMOC.

5. Summary and Discussion

In this paper, we first systematically evaluate how the CMIP5 models perform in reproducing the spatial and temporal variabilities of the NAO with special focus on multidecadal time scales. Then, we assess the simulated multidecadal NHT variability using the internal component extracted from the total variability. Finally, we analyze the model representation of the observed NAO-NHT relationship and explore possible sources of the model discrepancies.

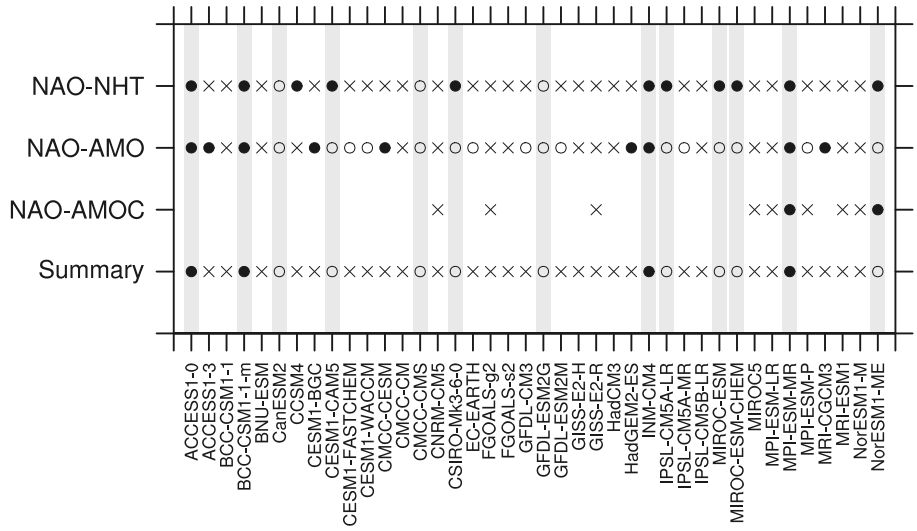

Figure 11. Summary of the CMIP5 model performance in reproducing the NAO-NHT, NAO-AMO, and NAO-AMOC linkages. In the first to third rows, a solid dot indicates that the model reproduces the significant positive correlation when the NAO precedes the NHT, AMO, and AMOC, respectively. A circle indicates that the model reproduces the positive correlation but not significant. Blank means the AMOC data of the model are not available. In the fourth row, a solid dot indicates that the model reproduces all the significant correlations in the above rows. A circle means that the model captures the above linkages but at least one of them is not significant. A cross indicates that the model fails to reproduce at least one of the considered linkages. The grey shading highlights the models that capture all the considered linkages.

We find that, in general, all of the models generate a reasonable representation of the seesaw structure in SLP changes related to the interannual NAO. Improvement is shown by the CMIP5 models in reproducing the spatial pattern of the NAO relative to the CMIP3 models. Nevertheless, there are still some biases in the location and amplitude of the centers of action. Most of the simulated Azores Highs are located to the northeast of the observed position, and nearly half of the Icelandic Lows show an eastward displacement. Compared with the interannual NAO pattern, there is less consistency between the modeled and observed decadal NAO patterns. The eastward bias of both pressure centers and the northward bias of the Azores High are more pronounced for the decadal NAO patterns. With respect to the temporal variability of the NAO, the simulated standard deviations of the annual mean NAOI are in good agreement with the observations, but the amplitudes of the decadal to multidecadal variabilities are underestimated by most of the models. Power spectrum analysis supports the conclusion that most of the models exhibit less variance over decadal and multidecadal scales than do the observations.

Regarding the simulation of the NHT, multidecadal variations of the twentieth century NHT that incorporate both internal and external forced variabilities are generally well captured by the CMIP5 models. However, this is mainly the result of the reasonable interpretation of the models concerning the forced part of the NHT variability. By subtracting the multimodel ensemble mean from the NHT time series simulated by each individual model, the unforced internal component of the NHT variability is isolated. We find that most of the CMIP5 models tend to underestimate the multidecadal fluctuation of the internal NHT. Based on observational studies, *Li et al*. [2013] found a 16 year phase lead of the NAO relative to the detrended NHT, which suggests that the NAO multidecadal variability is an important internal source of the multidecadal NHT. This connection between the NAO and hemispheric surface temperature variation is supported by modeling studies that provide further evidence of associated physical processes [*Delworth and Zeng*, 2016; *Delworth et al*., 2016]. Thus, it is reasonable to attribute the underestimation of the multidecadal variability of the internal NHT partially to the inadequate representation of the multidecadal fluctuation of the NAO by the models. However, the NAO is not the only driver of the multidecadal NHT variability; other possible factors such as the IPO [*Dai et al*., 2015; *Kosaka and Xie*, 2016] may also contribute to the model representation of the internal variability of NHT.

Model simulations of the observed NAO-NHT relationship are also examined. In the historical simulations, 14 models (ACCESS1-0, BCC-CSM1-1-m, CanESM2, CCSM4, CESM1-CAM5, CMCC-CMS, CSIRO-Mk3-6-0, GFDL-ESM2G, INM-CM4, IPSL-CM5A-LR, MIROC-ESM, MIROC-ESM-CHEM, MPI-ESM-MR, and NorESM1-ME) generally reproduce the positive correlation peak when the NAO leads the NHT by up to two decades, although with some biases in lag time and the significance of the correlation. Previous studies have suggested that the AMO acts as a "bridge" that passes the multidecadal NAO signal to the NHT [*Li et al*., 2013; *Sun et al*., 2015b]. Correspondingly, a delayed response of the North Atlantic SST to the NAO is also detected in all the models that reproduce the NAO's lead on the NHT, except CCSM4 (Figure 11). To explore the discrepancies in model simulations of the NAO-NHT connection, we classify the models into two categories based on whether they reproduce the delayed response of the NHT to the NAO. The models that capture the NAO's lead on the NHT also generate a delayed response of the AMOC to the NAO forcing, as well as the SST warming over the North Atlantic region associated with the enhanced AMOC. In contrast, these processes are not seen in models that fail to reproduce the NAO-NHT relationship. This indicates that capturing the slow ocean processes related to the AMOC may play an important role in the successful reproduction of the NAO-NHT connection. Although sampling variability may make a partial contribution to the discrepancies in the model simulations of the NAO-NHT connection, it is possible that the inconsistency between models is derived mainly from their different interpretation of the underlying physical processes.

In addition, to examine the consistency in the simulation of the NAO-NHT relationship between different runs of the same model, lead-lag correlations for the 10 ensemble members of CNRM-CM5 are calculated as an example. Large inconsistency in the correlation patterns is found among different runs (not shown). However, as in the first run, the significant decadal lead of the NAO on the NHT is not captured by the other runs. Since the NAO and the unforced NHT are mainly internally generated variabilities, there can be large differences in the simulated phases between different runs of the same model. The inconsistency in the simulated NAO-NHT correlations is a demonstration of the difference in the chronologies of the simulated NAO and NHT among different runs. Besides, this inconsistency is also an illustration of the uncertainties that lie in the analysis results concerning decadal relationships derived from relatively short time series. We must

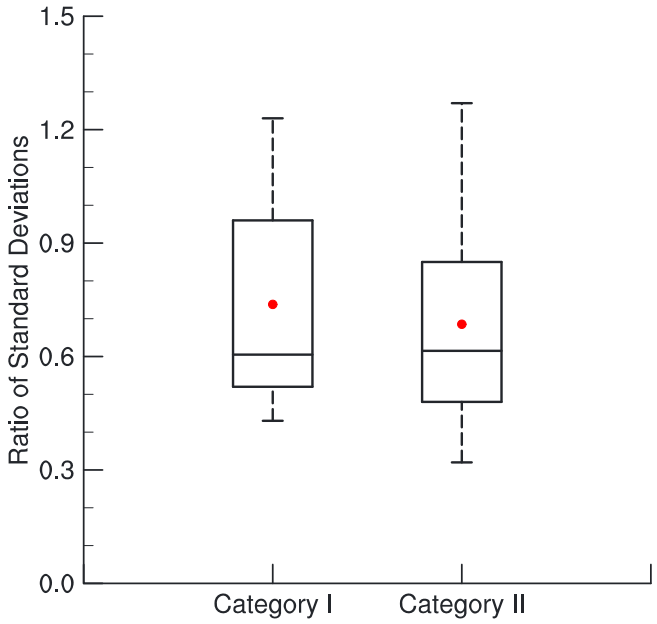

Figure 12. Distribution of the ratios of standard deviations between modeled and observed internal variabilities of the decadally smoothed NHT for Category I and Category II models. From top to bottom, horizontal bars in the box plot indicate the maximum, upper quartile, median, lower quartile, and minimum of the ratios. The red dot indicates the average value of the ratios.

point out that one limitation of this study lies in the relatively short time series used in the lead-lag correlation analysis. The historical simulations of the NAO-NHT and NAO-AMO relationship are based on data sets that cover periods of only about 100 years. Thus, the robustness of this relationship is difficult to confirm. One possible approach to tackling this problem is to further analyze this relationship using preindustrial control runs that cover a much longer time period. This would require a large amount of computing resources but could be considered in future studies.

Previous studies also found significant negative correlations when the NAO lags the AMO by up to 20 years [*Li et al*., 2013; *Peings and Magnusdottir*, 2014; *Sun et al*., 2015b], indicating a possible feedback from the AMO to the NAO after the NAO's delayed influence on the AMO. However, this significant lead-lag relationship between the NAO and the AMO is roughly generated by only a few of the models (CESM1-CAM5, CESM1-FASTCHEM, CSIRO-Mk3-6-0, GFDL-ESM2G, INM-CM4, MRI-CGCM3, and NorESM1-ME) considered in this study. Similarly, *Peings et al*. [2016] have also reported the lack of this lead-lag relationship between the NAO and the AMO in CMIP5 simulations and further analyzed the specific behavior of GFDL-ESM2G in reproducing the feedback of the AMO onto the NAO. The forcing effect from the NAO and the feedback from the ocean are two of the key processes responsible for the multidecadal fluctuation of the NAO [*Sun et al*., 2015b]. Thus, the lack of these two processes could be one possible explanation for the lack of the multidecadal NAO variability in the model simulations.

This study assesses the representation of the observed NAO-NHT linkage in the CMIP5 models, which may provide a new insight into possible approaches to improving the simulation of the internal NHT variability. As done in section 4, we divide the models into two categories. Category I includes the 14 models that basically reproduce the leading influence of the NAO on the NHT, whereas the other 26 models are included in Category II. Figure 12 displays the distribution of the ratios of standard deviations between simulated and observed decadally smoothed internal NHT anomalies for Category I and Category II models. Compared with the Category II models, Category I models generally give higher standard deviations, indicating that the multidecadal NHT variability is relatively less underestimated by these models. Thus, simulating the effect of the NAO on the NHT is important for representing natural variability of the NHT in the AOGCMs. To improve the model representation of the NHT, future efforts will be required in the simulation of the underlying physical processes associated with the leading influence of the NAO on the NHT.

Appendix A: Individual Performances of the 40 CMIP5 Models

Shown are the simulations of the individual CMIP5 models for the cross-correlation coefficients between regionally zonal-averaged SLPs over the North Atlantic region (Figure A1), the interannual NAO pattern (Figure A2), the decadal NAO pattern (Figure A3), and the lead-lag correlation coefficients between the NAOI and AMOI (Figure A4).

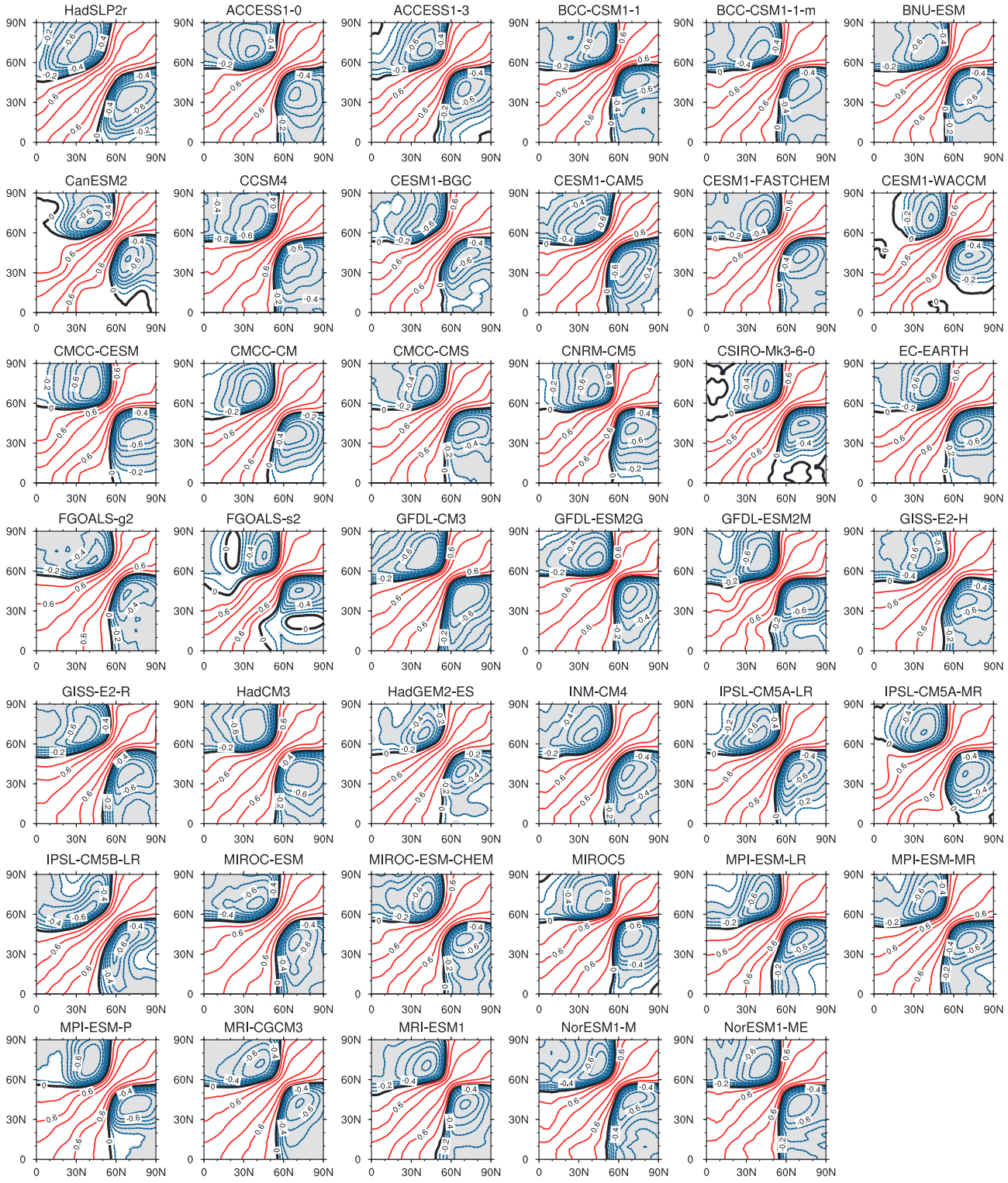

Figure A1. Cross-correlation coefficients between regionally zonal-averaged annual mean SLPs over the North Atlantic region (80°W–30°E) for the period 1900–2005 derived from HadSLP2r as well as CMIP5 models. The red solid (blue dashed) contours represent positive (negative) values at an interval of 0.3 (0.1), and the significant negative correlations at the 95% confidence level are shaded.

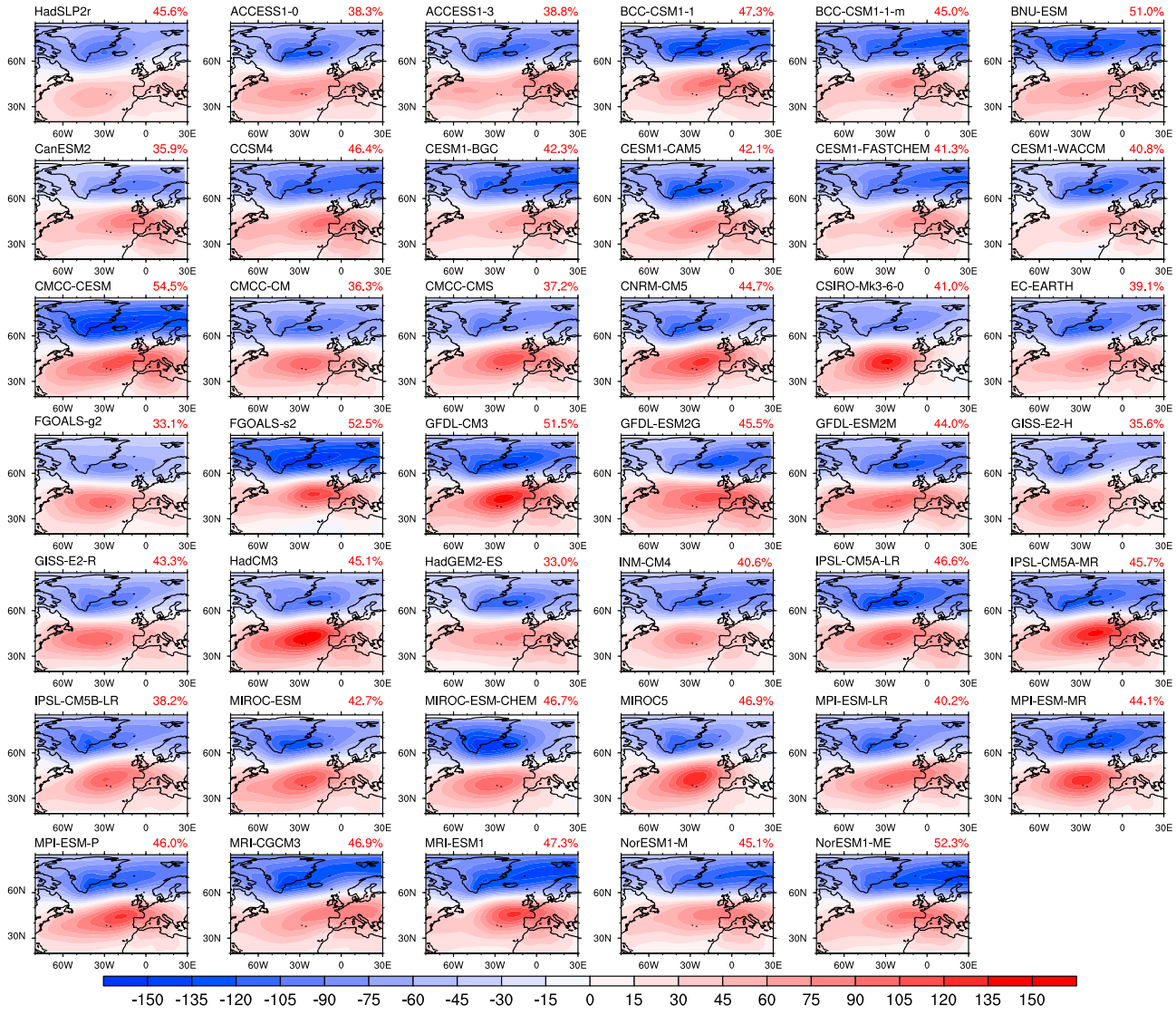

Figure A2. The leading EOF mode of annual mean SLP field over the North Atlantic sector derived from HadSLP2r and historical simulations of the CMIP5 models. The red numbers at the top right corner indicate the explained variance.

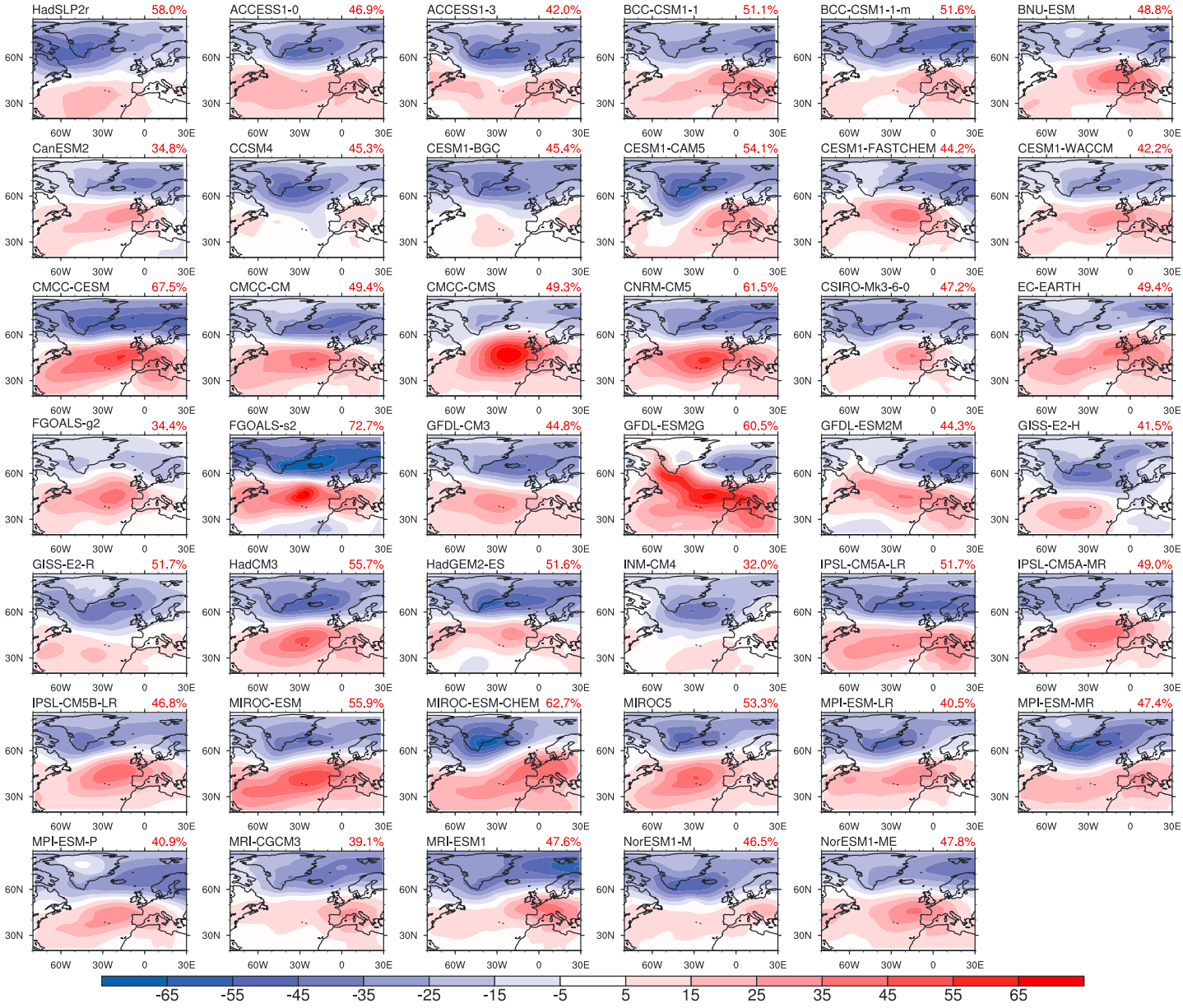

Figure A3. As in Figure A2 but for the result of decadally smoothed SLP. For INM-CM4, the second EOF mode is displayed.

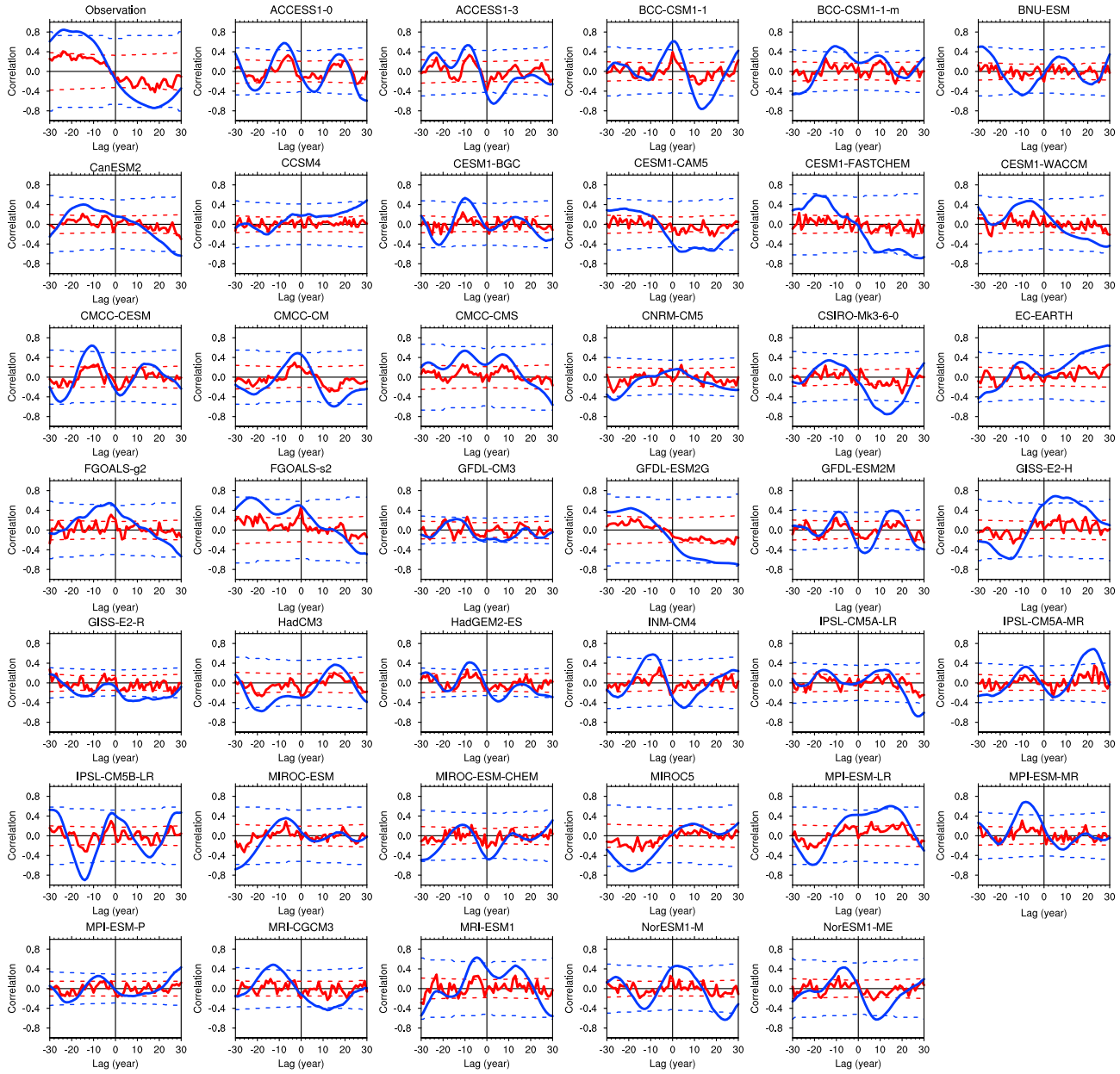

Figure A4. As in Figure 8 but for the lead-lag correlation coefficients between the NAOI and AMOI.

Acknowledgments
This work is jointly supported by the MOST key project (2016YFA0601801), National Natural Science Foundation of China (NSFC) project (41522502), and SOA International Cooperation Program on Global Change and Air-Sea Interactions (GASI-IPOVAI-03). We acknowledge the modeling groups listed in Table 1 for providing the model output for analysis, the WCRP's Working Group on Coupled Modelling (WGCM) for organizing the CMIP, and the Earth System Grid Federation (ESGF) for supporting the model data archive (http://cmip-pcmdi.llnl.gov/cmip5). The HadSLP2r, HadCRUT4, and HadSST3 data sets are obtained from the UK Met Office Hadley Centre and can be downloaded from http://www.metoffice.gov.uk/hadobs/hadslp2/, http://www.metoffice.gov.uk/hadobs/hadcrut4/ and http://www.metoffice.gov.uk/hadobs/hadsst3/, respectively. The NCAR SLP data set is available at the Climate Data Guide webpage at https://climatedataguide.ucar.edu/climate-data/ncar-sea-level-pressure. The 20CRv2c data set is provided by the NOAA/OAR/ESRL PSD, Boulder, Colorado, USA, from their website at http://www.esrl.noaa.gov/psd/. We also thank the three anonymous reviewers for their valuable comments and suggestions that help to greatly improve the manuscript.

References

Allan, R., and T. Ansell (2006), A new globally-complete monthly historical gridded mean sea level pressure dataset (HadSLP2): 1850–2004, *J. Clim.*, *19*(22), 5816–5842, doi:10.1175/JCLI3937.1.

Beckers, J. M., and M. Rixen (2003), EOF calculations and data filling from incomplete oceanographic datasets, *J. Atmos. Oceanic Technol.*, *20*(12), 1839–1856, doi:10.1175/1520-0426(2003)020<1839:Ecadff>2.0.Co;2.

Bladé, I., D. Fortuny, G. J. van Oldenborgh, and B. Liebmann (2012), The summer North Atlantic Oscillation in CMIP3 models and related uncertainties in projected summer drying in Europe, *J. Geophys. Res.*, *117*, D16104, doi:10.1029/2012JD017816.

Booth, B. B. B., N. J. Dunstone, P. R. Halloran, T. Andrews, and N. Bellouin (2012), Aerosols implicated as a prime driver of twentieth-century North Atlantic climate variability, *Nature*, *484*(7393), 228–232, doi:10.1038/nature10946.

Casado, M. J., and M. A. Pastor (2012), Use of variability modes to evaluate AR4 climate models over the Euro-Atlantic region, *Clim. Dyn.*, *38*(1–2), 225–237, doi:10.1007/s00382-011-1077-2.

Chung, C., and S. Nigam (1999), Weighting of geophysical data in principal component analysis, *J. Geophys. Res.*, *104*, 16,925–16,928, doi:10.1029/1999JD900234.

Compo, G. P., J. S. Whitaker, P. D. Sardeshmukh, N. Matsui, R. J. Allan, X. Yin, B. E. Gleason, R. S. Vose, G. Rutledge, and P. Bessemoulin (2011), The twentieth century reanalysis project, *Q. J. R. Meteorol. Soc.*, *137*(654), 1–28, doi:10.1002/qj.776.

Cook, E. R., R. D. D'Arrigo, and K. R. Briffa (1998), A reconstruction of the North Atlantic Oscillation using tree-ring chronologies from North America and Europe, *The Holocene*, *8*, 9–17, doi:10.1191/095968398677793225.

Dai, A., J. C. Fyfe, S.-P. Xie, and X. Dai (2015), Decadal modulation of global surface temperature by internal climate variability, *Nat. Clim. Change*, *5*(6), 555–559, doi:10.1038/NCLIMATE2605.

Davini, P., and C. Cagnazzo (2013), On the misinterpretation of the North Atlantic Oscillation in CMIP5 models, *Clim. Dyn.*, *43*(5–6), 1497–1511, doi:10.1007/s00382-013-1970-y.

Delworth, T. L., and R. J. Greatbatch (2000), Multidecadal thermohaline circulation variability driven by atmospheric surface flux forcing, *J. Clim.*, *13*(9), 1481–1495, doi:10.1175/1520-0442(2000)013<1481:MTCVDB>2.0.CO;2.

Delworth, T. L., and M. E. Mann (2000), Observed and simulated multidecadal variability in the Northern Hemisphere, *Clim. Dyn.*, *16*(9), 661–676, doi:10.1007/s003820000075.

Delworth, T. L., and F. Zeng (2016), The impact of the North Atlantic Oscillation on climate through its influence on the Atlantic meridional overturning circulation, *J. Clim.*, *29*(3), 941–962, doi:10.1175/JCLI-D-15-0396.1.

Delworth, T. L., F. Zeng, G. A. Vecchi, X. Yang, L. Zhang, and R. Zhang (2016), The North Atlantic Oscillation as a driver of rapid climate change in the Northern Hemisphere, *Nat. Geosci.*, *9*(7), 509–512, doi:10.1038/NGEO2738.

Deser, C., and H. Teng (2008), Evolution of Arctic sea ice concentration trends and the role of atmospheric circulation forcing, 1979–2007, *Geophys. Res. Lett.*, *35*, L02504, doi:10.1029/2007GL032023.

Deser, C., J. W. Hurrell, and A. S. Phillips (2016), The role of the North Atlantic Oscillation in European climate projections, *Clim. Dyn.*, *79*(3–4), 231–244, doi:10.1007/s00382-016-3502-z.

Ding, R. Q., J. P. Li, S. Wang, and F. Ren (2005), Decadal change of the spring dust storm in northwest China and the associated atmospheric circulation, *Geophys. Res. Lett.*, *32*, L02808, doi:10.1029/2004GL021561.

Eden, C., and T. Jung (2001), North Atlantic interdecadal variability: Oceanic response to the North Atlantic Oscillation (1865-1997), *J. Clim.*, *14*(5), 676–691, doi:10.1175/1520-0442(2001)014<0676:NAIVOR>2.0.CO;2.

Flato, G., et al. (2013), Evaluation of climate models, in *Climate Change 2013: The Physical Science Basis. Contribution of Working Group I to the Fifth Assessment Report of the Intergovernmental Panel on Climate Change*, edited by T. F. Stocker et al., pp. 741–866, Cambridge Univ. Press, Cambridge, U. K., and New York, doi:10.1017/CBO9781107415324.

Gámiz-Fortis, S. R., D. Pozo-Vázquez, M. J. Esteban-Parra, and Y. Castro-Díez (2002), Spectral characteristics and predictability of the NAO assessed through Singular Spectral Analysis, *J. Geophys. Res.*, *107*(D23), 4685, doi:10.1029/2001JD001436.

Gillett, N. P., and J. C. Fyfe (2013), Annular mode changes in the CMIP5 simulations, *Geophys. Res. Lett.*, *40*, 1189–1193, doi:10.1002/grl.50249.

Gong, D.-Y., S.-W. Wang, and J.-H. Zhu (2001), East Asian winter monsoon and Arctic Oscillation, *Geophys. Res. Lett.*, *28*(10), 2073–2076, doi:10.1029/2000GL012311.

Handorf, D., and K. Dethloff (2012), How well do state-of-the-art atmosphere-ocean general circulation models reproduce atmospheric teleconnection patterns?, *Tellus A*, *64*, 19777, doi:10.3402/tellusa.v64i0.19777.

Hurrell, J. W. (1995), Decadal trends in the North Atlantic Oscillation: Regional temperatures and precipitation, *Science*, *269*(5224), 676–679, doi:10.1126/science.269.5224.676.

Hurrell, J. W., and H. Van Loon (1997), Decadal variations in climate associated with the North Atlantic Oscillation, *Clim. Change*, *36*(3–4), 301–326, doi:10.1023/A:1005314315270.

Hurrell, J. W., Y. Kushnir, G. Ottersen, and M. Visbeck (2003), An overview of the North Atlantic Oscillation, in *The North Atlantic Oscillation: Climatic Significance and Environmental Impact*, edited by J. W. Hurrell et al., pp. 1–35, AGU, Washington, D. C., doi:10.1029/134GM01.

Jones, G. S., P. A. Stott, and N. Christidis (2013), Attribution of observed historical near-surface temperature variations to anthropogenic and natural causes using CMIP5 simulations, *J. Geophys. Res. Atmos.*, *118*, 4001–4024, doi:10.1002/jgrd.50239.

Keenlyside, N. S., M. Latif, J. Jungclaus, L. Kornblueh, and E. Roeckner (2008), Advancing decadal-scale climate prediction in the North Atlantic sector, *Nature*, *453*(7191), 84–88, doi:10.1038/nature06921.

Kennedy, J. J., N. A. Rayner, R. O. Smith, D. E. Parker, and M. Saunby (2011a), Reassessing biases and other uncertainties in sea surface temperature observations measured in situ since 1850: 1. Measurement and sampling uncertainties, *J. Geophys. Res.*, *116*, D14103, doi:10.1029/2010JD015218.

Kennedy, J. J., N. A. Rayner, R. O. Smith, D. E. Parker, and M. Saunby (2011b), Reassessing biases and other uncertainties in sea surface temperature observations measured in situ since 1850: 2. Biases and homogenization, *J. Geophys. Res.*, *116*, D14104, doi:10.1029/2010JD015220.

Knight, J. R. (2009), The Atlantic Multidecadal Oscillation inferred from the forced climate response in coupled general circulation models, *J. Clim.*, *22*(7), 1610–1625, doi:10.1175/2008JCLI2628.1.

Knight, J. R., R. J. Allan, C. K. Folland, M. Vellinga, and M. E. Mann (2005), A signature of persistent natural thermohaline circulation cycles in observed climate, *Geophys. Res. Lett.*, *32*, L20708, doi:10.1029/2005GL024233.

Knutson, T. R., F. Zeng, and A. T. Wittenberg (2013), Multimodel assessment of regional surface temperature trends: CMIP3 and CMIP5 twentieth-century simulations, *J. Clim.*, *26*(22), 8709–8743, doi:10.1175/JCLI-D-12-00567.1.

Kondrashov, D., and M. Ghil (2006), Nonlinear processes in geophysics spatio-temporal filling of missing points in geophysical data sets, *Nonlinear Processes Geophys.*, *13*, 151–159, doi:10.5194/npg-13-151-2006.

Kosaka, Y., and S.-P. Xie (2016), The tropical Pacific as a key pacemaker of the variable rates of global warming, *Nat. Geosci.*, *9*(9), 669–673, doi:10.1038/NGEO2770.
Kravtsov, S., and C. Spannagle (2008), Multidecadal climate variability in observed and modeled surface temperatures, *J. Clim.*, *21*(5), 1104–1121, doi:10.1175/2007JCLI1874.1.
Latif, M., C. Böning, J. Willebrand, A. Biastoch, J. Dengg, N. Keenlyside, U. Schweckendiek, and G. Madec (2006a), Is the thermohaline circulation changing?, *J. Clim.*, *19*(18), 4631–4637, doi:10.1175/JCLI3876.1.
Latif, M., M. Collins, H. Pohlmann, and N. Keenlyside (2006b), A review of predictability studies of Atlantic sector climate on decadal time scales, *J. Clim.*, *19*(23), 5971–5987, doi:10.1175/JCLI3945.1.
Lee, Y. Y., and R. X. Black (2013), Boreal winter low-frequency variability in CMIP5 models, *J. Geophys. Res. Atmos.*, *118*, 6891–6904, doi:10.1002/jgrd.50493.
Li, J. P. (2005), Coupled air-sea oscillations and climate variations in China, in *Climate and Environmental Evolution in China (First Volume)*, edited by D. Qin, pp. 324–333, China Meteorol. Press, Beijing.
Li, J. P., and J. X. L. Wang (2003), A new North Atlantic Oscillation index and its variability, *Adv. Atmos. Sci.*, *20*(5), 661–676.
Li, J. P., C. Sun, and F. F. Jin (2013), NAO implicated as a predictor of Northern Hemisphere mean temperature multidecadal variability, *Geophys. Res. Lett.*, *40*, 5497–5502, doi:10.1002/2013GL057877.
Liu, T., J. P. Li, J. Feng, X. Wang, and Y. Li (2016), Cross-seasonal relationship between the boreal autumn SAM and winter precipitation in the Northern Hemisphere in CMIP5, *J. Clim.*, *29*(18), 6617–6636, doi:10.1175/JCLI-D-15-0708.1.
Mann, M. E., B. A. Steinman, and S. K. Miller (2014), On forced temperature changes, internal variability, and the AMO, *Geophys. Res. Lett.*, *41*, 3211–3219, doi:10.1002/2014GL059233.
Marshall, J., Y. Kushnir, D. Battisti, P. Chang, A. Czaja, R. Dickson, J. Hurrell, M. McCartny, R. Saravanan, and M. Visbeck (2001), North Atlantic climate variability: Phenomena, impacts and mechanisms, *Int. J. Climatol.*, *21*(15), 1863–1898, doi:10.1002/joc.693.
Mazzarella, A., and N. Scafetta (2012), Evidences for a quasi 60-year North Atlantic Oscillation since 1700 and its meaning for global climate change, *Theor. Appl. Climatol.*, *107*(3–4), 599–609, doi:10.1007/s00704-011-0499-4.
Morice, C. P., J. J. Kennedy, N. A. Rayner, and P. D. Jones (2012), Quantifying uncertainties in global and regional temperature change using an ensemble of observational estimates: The HadCRUT4 data set, *J. Geophys. Res.*, *117*, D08101, doi:10.1029/2011JD017187.
North, G. R., T. L. Bell, and R. F. Cahalan (1982), Sampling errors in the estimation of empirical orthogonal functions, *Mon. Weather Rev.*, *110*(7), 699–706, doi:10.1175/1520-0493(1982)110<0699:SEITEO>2.0.CO;2.
Olsen, J., N. J. Anderson, and M. F. Knudsen (2012), Variability of the North Atlantic Oscillation over the past 5,200 years, *Nat. Geosci.*, *5*(11), 808–812, doi:10.1038/ngeo1589.
Park, W., and M. Latif (2010), Pacific and Atlantic multidecadal variability in the Kiel climate model, *Geophys. Res. Lett.*, *37*, L24702, doi:10.1029/2010GL045560.
Peings, Y., and G. Magnusdottir (2014), Forcing of the wintertime atmospheric circulation by the multidecadal fluctuations of the North Atlantic Ocean, *Environ. Res. Lett.*, *9*(3), doi:10.1088/1748-9326/9/3/034018.
Peings, Y., G. Simpkins, and G. Magnusdottir (2016), Multidecadal fluctuations of the North Atlantic Ocean and feedback on the winter climate in CMIP5 control simulations, *J. Geophys. Res. Atmos.*, *121*, 2571–2592, doi:10.1002/2015JD024107.
Pyper, B. J., and R. M. Peterman (1998), Comparison of methods to account for autocorrelation in correlation analyses of fish data, *Can. J. Fish. Aquat. Sci.*, *55*(9), 2127–2140, doi:10.1139/f98-201.
Schlesinger, M. E., and N. Ramankutty (1994), An oscillation in the global climate system of period 65–70 years, *Nature*, *367*(6465), 723–726, doi:10.1038/367723a0.
Schmidt, G. A., D. T. Shindell, and K. Tsigaridis (2014), Reconciling warming trends, *Nat. Geosci.*, *7*(3), 158–160.
Stoner, A. M. K., K. Hayhoe, and D. J. Wuebbles (2009), Assessing general circulation model simulations of atmospheric teleconnection patterns, *J. Clim.*, *22*(16), 4348–4372, doi:10.1175/2009JCLI2577.1.
Stott, P. A., S. F. Tett, G. S. Jones, M. R. Allen, J. F. Mitchell, and G. J. Jenkins (2000), External control of 20th century temperature by natural and anthropogenic forcings, *Science*, *290*(5499), 2133–2137, doi:10.1126/science.290.5499.2133.
Sun, C., J. P. Li, J. Feng, and F. Xie (2015a), A decadal-scale teleconnection between the North Atlantic Oscillation and subtropical eastern Australian rainfall, *J. Clim.*, *28*(3), 1074–1092, doi:10.1175/JCLI-D-14-00372.1.
Sun, C., J. P. Li, and F. F. Jin (2015b), A delayed oscillator model for the quasi-periodic multidecadal variability of the NAO, *Clim. Dyn.*, *45*(7–8), 2083–2099, doi:10.1007/s00382-014-2459-z.
Sutton, R. T., and D. L. Hodson (2005), Atlantic Ocean forcing of North American and European summer climate, *Science*, *309*(5731), 115–118, doi:10.1126/science.1109496.
Swanson, K. L., G. Sugihara, and A. A. Tsonis (2009), Long-term natural variability and 20th century climate change, *Proc. Natl. Acad. Sci. U.S.A.*, *106*(38), 16,120–16,123, doi:10.1073/pnas.0908699106.
Tandon, N. F., and P. J. Kushner (2015), Does external forcing interfere with the AMOC's influence on North Atlantic sea surface temperature?, *J. Clim.*, *28*(16), 6309–6323, doi:10.1175/JCLI-D-14-00664.1.
Taylor, K. E. (2001), Summarizing multiple aspects of model performance in a single diagram, *J. Geophys. Res.*, *106*(D7), 7183–7192, doi:10.1029/2000JD900719.
Taylor, K. E., R. J. Stouffer, and G. A. Meehl (2012), An overview of CMIP5 and the experiment design, *Bull. Am. Meteorol. Soc.*, *93*(4), 485–498, doi:10.1175/BAMS-D-11-00094.1.
Thompson, D. W., and J. M. Wallace (2001), Regional climate impacts of the Northern Hemisphere annular mode, *Science*, *293*(5527), 85–89, doi:10.1126/science.1058958.
Trenberth, K. E., and D. A. Paolino Jr. (1980), The Northern Hemisphere sea-level pressure data set: Trends, errors and discontinuities, *Mon. Weather Rev.*, *108*(7), 855–872, doi:10.1175/1520-0493(1980)108<0855:TNHSLP>2.0.CO;2.
Wanner, H., S. Brönnimann, C. Casty, D. Gyalistras, J. Luterbacher, C. Schmutz, D. B. Stephenson, and E. Xoplaki (2001), North Atlantic Oscillation—Concepts and studies, *Surv. Geophys.*, *22*(4), 321–382, doi:10.1023/A:1014217317898.
Wilks, D. S. (2006), Principal component (EOF) analysis, in *Statistical Methods in the Atmospheric Sciences*, pp. 463–507, Academic Press, San Diego, Calif.
Woollings, T., C. Franzke, D. L. R. Hodson, B. Dong, E. A. Barnes, C. C. Raible, and J. G. Pinto (2015), Contrasting interannual and multidecadal NAO variability, *Clim. Dyn.*, *45*(1–2), 539–556, doi:10.1007/s00382-014-2237-y.
Wu, Z. W., B. Wang, J. P. Li, and F. F. Jin (2009), An empirical seasonal prediction model of the east Asian summer monsoon using ENSO and NAO, *J. Geophys. Res.*, *114*, D18120, doi:10.1029/2009JD011733.
Wu, Z. W., J. P. Li, Z. Jiang, J. He, and X. Zhu (2012), Possible effects of the North Atlantic Oscillation on the strengthening relationship between the east Asian summer monsoon and ENSO, *Int. J. Climatol.*, *32*(5), 794–800, doi:10.1002/joc.2309.

Wunsch, C. (1999), The interpretation of short climate records, with comments on the North Atlantic and Southern oscillations, *Bull. Am. Meteorol. Soc.*, *80*(2), 245–255, doi:10.1175/1520-0477(1999)080<0245:TIOSCR>2.0.CO;2.

Wyatt, M. G., S. Kravtsov, and A. A. Tsonis (2012), Atlantic Multidecadal Oscillation and Northern Hemisphere's climate variability, *Clim. Dyn.*, *38*(5–6), 929–949, doi:10.1007/s00382-011-1071-8.

Xie, F., J. P. Li, W. Tian, X. Zhou, and X. Ma (2016), The variations in middle and upper stratospheric water vapour over the past two decades, *SOLA*, *12*, 127–134, doi:10.2151/sola.2016-028.

Zhang, R., T. L. Delworth, and I. M. Held (2007), Can the Atlantic Ocean drive the observed multidecadal variability in Northern Hemisphere mean temperature?, *Geophys. Res. Lett.*, *34*, L02709, doi:10.1029/2006GL028683.

Zheng, F., J. P. Li, R. T. Clark, and H. C. Nnamchi (2013), Simulation and projection of the Southern Hemisphere annular mode in CMIP5 models, *J. Clim.*, *26*(24), 9860–9879, doi:10.1175/JCLI-D-13-00204.1.

Zheng, F., J. P. Li, Y. Li, S. Zhao, and D. Deng (2016), Influence of the summer NAO on the spring-NAO-based predictability of the East Asian summer monsoon, *J. Appl. Meteorol. Climatol.*, *55*(7), 1459–1476, doi:10.1175/JAMC-D-15-0199.1.

Zhou, T., and R. Yu (2006), Twentieth-century surface air temperature over China and the globe simulated by coupled climate models, *J. Clim.*, *19*(22), 5843–5858, doi:10.1175/JCLI3952.1.